

University of Windsor

## Scholarship at UWindor

---

Electronic Theses and Dissertations

Theses, Dissertations, and Major Papers

---

1-1-1968

### A study of the EPR spectrum of the calcium hydroxide:manganese system as a function of temperature.

Stuart M. Quick  
*University of Windsor*

Follow this and additional works at: <https://scholar.uwindsor.ca/etd>

---

#### Recommended Citation

Quick, Stuart M., "A study of the EPR spectrum of the calcium hydroxide:manganese system as a function of temperature." (1968). *Electronic Theses and Dissertations*. 6060.

<https://scholar.uwindsor.ca/etd/6060>

This online database contains the full-text of PhD dissertations and Masters' theses of University of Windsor students from 1954 forward. These documents are made available for personal study and research purposes only, in accordance with the Canadian Copyright Act and the Creative Commons license—CC BY-NC-ND (Attribution, Non-Commercial, No Derivative Works). Under this license, works must always be attributed to the copyright holder (original author), cannot be used for any commercial purposes, and may not be altered. Any other use would require the permission of the copyright holder. Students may inquire about withdrawing their dissertation and/or thesis from this database. For additional inquiries, please contact the repository administrator via email ([scholarship@uwindsor.ca](mailto:scholarship@uwindsor.ca)) or by telephone at 519-253-3000ext. 3208.

A STUDY OF THE EPR SPECTRUM OF THE  $\text{Ca}(\text{OH})_2:\text{Mn}^{2+}$   
SYSTEM AS A FUNCTION OF TEMPERATURE

by

Stuart M. Quick

A Dissertation  
Submitted to the Faculty of Graduate Studies through the Department  
of Physics in Partial Fulfillment of the Requirements for  
the Degree of Doctor of Philosophy at the  
University of Windsor

Windsor, Ontario

1968

UMI Number: DC52625

### INFORMATION TO USERS

The quality of this reproduction is dependent upon the quality of the copy submitted. Broken or indistinct print, colored or poor quality illustrations and photographs, print bleed-through, substandard margins, and improper alignment can adversely affect reproduction.

In the unlikely event that the author did not send a complete manuscript and there are missing pages, these will be noted. Also, if unauthorized copyright material had to be removed, a note will indicate the deletion.

**UMI**<sup>®</sup>

---

UMI Microform DC52625

Copyright 2008 by ProQuest LLC.

All rights reserved. This microform edition is protected against unauthorized copying under Title 17, United States Code.

ProQuest LLC  
789 E. Eisenhower Parkway  
PO Box 1346  
Ann Arbor, MI 48106-1346

APX 6521

APPROVED BY:

Yeung Wook Kim  
NEHedgecock

F. Holy

E. Alsd

223850

ABSTRACT

The electron paramagnetic resonance (EPR) spectrum of  $Mn^{2+}$  impurity in synthetic crystals of  $Ca(OH)_2$  was studied as a function of temperature in the range  $85^\circ K$ - $800^\circ K$  at x-band microwave frequencies. The spectrum was fitted to the following spin-Hamiltonian which is invariant in  $D_{3d}$  symmetry.

$$H(s) = \beta \vec{H} \cdot \vec{g} \cdot \vec{S} + \vec{I} \cdot \vec{A} \cdot \vec{S} + \frac{1}{3} b_2^0 S_2^2 + \frac{1}{60} b_4^0 S_4^2 + \frac{1}{60} b_4^3 S_4^3$$

At RT( $290^\circ K$ ) the following values were obtained for the parameters:

$$\begin{aligned} g_{11} &= 2.0011 \pm 0.0005 & g_{\perp} &= 2.0010 \pm 0.0005 & b_2^0 &= -6.7 \pm 0.5G \\ b_4^0 &= -2.48 \pm 0.25G & b_4^3 &= 0 \pm 100G \\ A &= -92.05 \pm 0.15G & B &= -90.28 \pm 0.15G \end{aligned}$$

The value of  $b_2^0(0) = -14.25G$  which was predicted by the static theory of Sharma, Das, and Orbach,<sup>33,34</sup> was in good agreement with the value  $b_2^0(0) = -16.25G$  which was extrapolated from the experimental data. The temperature dependence of the experimental  $b_2^0$ , however, differed markedly from the dependence predicted by this theory when the effect of thermal expansion was taken into account. The following curve was fitted to the data:

$$b_2^0(T) = (b_2^0)_0 + 4.97 \times 10^{-42} K_1 \coth\left(\frac{196}{T}\right) + 11.3 \times 10^{-42} K_2 \coth\left(\frac{172}{T}\right)$$

where  $(b_2^0)_0 = -21.5 \pm 0.5G$ ,  $K_1 = (-5.38 \pm 0.5) \times 10^{42} G/erg\text{-sec}^2$ , and  $K_2 = (2.83 \pm 0.5) \times 10^{42} G/erg\text{-sec}^2$ . This curve was obtained on the basis of the theory of Walsh, Jeener and Bloembergen<sup>37</sup> by assuming that two  $T'$  lattice modes transforming as  $A_{1g}$  and  $E_g$  under  $D_{3d}$  symmetry were responsible for the  $Mn^{2+}$

vibronic coupling. The possibility of explaining  $b_2^0(T)$  on the basis of a Debye frequency spectrum is also pointed out in the text.

The temperature dependence of  $b_4^0$  was approximately linear. Therefore, the effects of lattice vibrations on this quantity were probably negligible. Although the data tended to support a dependence, such as  $b_4^0 = CR_0^{-n}$ , where  $C$  is a constant,  $R_0$  is the Ca-O bond distance, and  $n$  is a number, it proved impossible to determine  $n$  accurately.

The theory of Simanek and Orbach<sup>50</sup> was used to describe the temperature dependence of the isotropic Fermi contact hyperfine tensor.

A curve of the form

$$A(T) = A(0) \left[ 1 - CT^4 \int_0^{\theta/T} \frac{x^3 dx}{e^x - 1} \right]$$

was fitted to the data. The best fit was obtained for  $A(0) = -92.00G$ ,  $C = 1.78 \times 10^{-12} \text{ } ^\circ K^{-4}$ , and a Debye Temperature of  $\theta = 500^\circ K$ . The quantity  $\eta = \left| \frac{(A^2 - B^2)^{1/2}}{A} \right|$  decreased at a rate of the order of  $7.6 \times 10^{-5} \text{ } ^\circ K^{-1}$ .

$Mn^{2+}$ -H SHFS was observed in the range  $85^\circ K$ - $130^\circ K$ .

The interaction was highly isotropic. The isotropic Fermi contact HFS tensor was of the order of  $4.5G$  at  $85^\circ K$ . The anisotropic dipolar HFS tensor was probably of the order of  $0.1G$  or less. A dependence of the SHFS on  $M_s$  was also noted, but no theoretical explanation was given.

#### ACKNOWLEDGEMENTS

The author wishes to thank Dr. F. Holuj for first suggesting this problem and for his guidance and encouragement during the course of the work. Thanks are due to Mr. W. Grewe and the machine shop staff for construction of apparatus. Financial assistance in the form of a Province of Ontario Graduate Fellowship is gratefully acknowledged.

TABLE OF CONTENTS

	Page
ABSTRACT	iii
ACKNOWLEDGEMENTS	iv
LIST OF TABLES	viii
LIST OF FIGURES	ix
CHAPTER	
I. INTRODUCTION AND PURPOSE OF THE EXPERIMENT	1
II. PHYSICAL PROPERTIES OF $\text{Ca}(\text{OH})_2$ CRYSTAL	3
Crystallography	3
Lattice Dynamics	6
III. THEORY	10
Crystal Field Theory of the $\text{Mn}^{2+}$ Ion	
The Hamiltonian Formalism as Applied to $\text{Mn}^{2+}$ in $\text{Ca}(\text{OH})_2$	11
Calculation of Spin-Hamiltonian Parameters	14
Crystal field parameters and g-values	14
Static splittings: the point-multipole model	14
Dynamic splittings: effects of lattice vibrations	18
Hyperfine structure parameters A and B	23
Static splittings: core polarization	23
Dynamic splittings: the orbit-lattice interaction	24
Superhyperfine structure Parameters	25
IV. INSTRUMENTATION AND CRYSTAL PREPARATION	27
V. EXPERIMENTAL PROCEDURE AND RESULTS	34
Analysis of the RT Spectrum	34
The FS and HFS Spectrum as a Function of Temperature	43
Temperature dependence of the crystal field parameters	45

	page
Temperature dependence of the hyperfine parameters	49
$Mn^{2+}$ -H SHFS and General Discussion of Lineshapes	49
VI. DISCUSSION AND CONCLUSIONS	58
REFERENCES	62
APPENDIX A. Proton MR Frequencies Obtained in Calibration of Magnetic Field Across 6 in. Gap of Varian Magnet	65
APPENDIX B. Best Fit Data of Spin-Hamiltonian Parameters $b_2^0, b_4^0,$ A and B, and the Quantities $ \frac{(A^2-B^2)^{1/2}}{A} $ and $(A+2B)/3$ in Gauss as a function of Temperature	66
VITA AUCTORIS	68

LIST OF TABLES

	Page
II.I Structural and other Data for $\text{Ca}(\text{OH})_2$ Crystal	5
II.II Types of Modes for $\text{Ca}(\text{OH})_2$ Crystal	9
II.III Fundamental T' Mode Frequencies	9
III.I $^6\text{S}$ State Splitting Mechanisms within PM Model	16
V.I Position of Resonant Fields at Room Temperature and for Microwave Frequency 9380 MHz.	37

## LIST OF FIGURES

		Page
II.1	Structure of $\text{Ca}(\text{OH})_2$ Projected on (0001) Plane	4
II.2	Nearest- and Next Nearest-Neighbour Environment of Calcium Atom in $\text{Ca}(\text{OH})_2$	4
II.3	T' Optical Modes of Vibration of $\text{Ca}(\text{OH})_2$ Crystal for $\vec{k}=0$	7
II.4	The First Brillouin Zone of the Trigonal Lattice	7
IV.1a	$\text{LN}_2$ -RT Variable Temperature Cavity	28
IV.1b	RT-800°K Variable Temperature Cavity	29
IV.2	Diffusion Box Used in Growing $\text{Ca}(\text{OH})_2$ Crystals	33
V.1a	Angular Variation of Spectrum for Rotation of $\vec{H}$ in (10 $\bar{1}$ 0) Plane	35
V.1b	Angular Variation of Spectrum for Rotation of $\vec{H}$ in ( $\bar{1}$ 2 $\bar{1}$ 0) Plane	36
V.2	Typical Recordings of the Spectrum at $T = 96^\circ\text{K}$	39
V.3	Typical Recordings of the Spectrum at RT	40
V.4	Typical Recordings of the Spectrum at $T = 609^\circ\text{K}$	41
V.5	Recordings of the Spectrum at $T = 825^\circ\text{K}$	44
V.6	$b_2^0$ vs. Temperature	46
V.7	$b_4^0$ vs. Temperature	47
V.8	A and B vs. Temperature	50
V.9	$\eta = \left  \frac{(A^2 - B^2)^{1/2}}{A} \right $ vs. Temperature	51
V.10	$(A+2B)/3$ vs. Temperature	52
V.11	FS Components of the $m=+5/2$ Hyperfine Line	53
V.12	The $M_s: \frac{1}{2} \leftrightarrow \frac{3}{2}; m = -5/2$ Line at Low and High Power Levels	55
V.13	Angular Variation of SHFS Splitting Relative to the Central Component	57

## CHAPTER I

### INTRODUCTION AND PURPOSE OF THE EXPERIMENT

Iron group ions with  $d^5$  configurations, e.g.,  $Mn^{2+}$  and  $Fe^{3+}$ , and rare-earth group ions with  $f^7$  configurations, e.g.,  $Gd^{3+}$  and  $Eu^{2+}$ , have S ground states in Russell-Saunders coupling. Any degeneracy remaining in the state is due to spin only. It has been observed that this spin degeneracy is partially removed when the ions are present in a crystalline environment. In recent years there has been much interest in explaining such S-state splittings theoretically.

Most of the mechanisms which have been proposed to explain S-state splittings are based on a rigid lattice model. These calculations reveal that the total S-state splitting can be the result of so-called crystal field interactions, hyperfine interactions, and sometimes, super-hyperfine interactions. These interactions are discussed in detail in Chapter III. In order to determine the contribution of each of these interactions to the total splitting, one computes the magnitude of the corresponding tensor (sometimes called parameter) in the spin-Hamiltonian. The spin-Hamiltonian for the  $Ca(OH)_2:Mn^{2+}$  system is introduced also in Chapter III. Walsh et. al.<sup>37</sup>, in 1965, studied experimentally the temperature dependence of the so-called axial crystal field parameter (D), the cubic crystal field parameter (a), and the hyperfine parameter (A), of paramagnetic ions in cubic crystals, such as MgO. These workers found that the temperature dependences of D and a could be explained by the

effects of thermal expansion on a mechanism based on the rigid lattice model. The temperature dependence of  $A$ , however, could not be so explained. They proposed that the temperature dependence of  $A$  was determined mainly by the effects of lattice vibrations, and that this dependence could have been computed explicitly had the phonon spectrum of the crystal been known. Simanek and Orbach<sup>50</sup>, in 1966, presented quantitative calculations of a mechanism which successfully describes the temperature dependence of the hyperfine parameter  $A$  of  $\text{Mn}^{2+}$  in cubic crystals.

The primary purpose of this experiment was to extend experimental studies of the type discussed above to  $\text{Mn}^{2+}$  in trigonal symmetry, in an environment only slightly less symmetrical than cubic. We chose to study the  $\text{Ca}(\text{OH})_2:\text{Mn}^{2+}$  system because it has a simple structure of the desired symmetry and because we were successful in introducing  $\text{Mn}^{2+}$  into the alkaline surroundings. The third reason was that the phonon spectrum of this crystal has been extensively studied. It was our intention to use such data to study the effect of Ca-OH vibrations on the temperature dependences of the spin-Hamiltonian parameters and to seek evidence of effects of internal OH vibrations on the superhyperfine structure at low temperatures.

## CHAPTER II

### PHYSICAL PROPERTIES OF $\text{Ca}(\text{OH})_2$ CRYSTAL

#### I. CRYSTALLOGRAPHY

X-ray studies<sup>1-9</sup> have shown  $\text{Ca}(\text{OH})_2$  to be of the hexagonal ( $\text{CdI}_2$ ) type with space group  $P \bar{3} 2/m 1 (D_{3d}^3)$ . A projection of the close-packed structure established by the X-ray studies is shown in Fig. II. 1. The Ca atoms lie in the invariant positions  $(0,0,0)$ , with point symmetry  $\bar{3}m$ , and the oxygen and hydrogen atoms lie in the special positions  $\pm(1/3, 2/3, z_o)$  and  $\pm(1/3, 2/3, z_h)$  respectively, both with point symmetry  $3m$ . The unit cell contains one molecule. The hydrogen positions, which could not be determined from the early X-ray work, were first postulated by Bernal and Megaw<sup>3</sup>. These positions have since been confirmed by X-ray diffraction<sup>7,8</sup>, neutron diffraction<sup>10</sup>, and nuclear magnetic resonance<sup>11</sup>.

The  $\text{Ca}(\text{OH})_2$  structure consists of layers of two sheets of hydroxyls parallel to the basal plane  $(0001)$ , with a sheet of Ca atoms between them. Each Ca atom lies between six OH groups forming an octahedron which is slightly compressed along  $[0001]$ . The layers are held together by weak Van der Waals' forces between the opposed hydroxyl sheets. Neutron diffraction studies reveal that the hydrogen motion is confined mainly to the hydrogen layers normal to the c axis. Consequently, there are no hydrogen bonds. This is supported by the observed softness (2 on Moh's scale) and perfect cleavage in the basal plane. The H motion is apparently very anharmonic<sup>15,10</sup>.

Structural data are collected in Table II.I. Fig. II. 2 shows in perspective the nearest- and second nearest-neighbour environment of

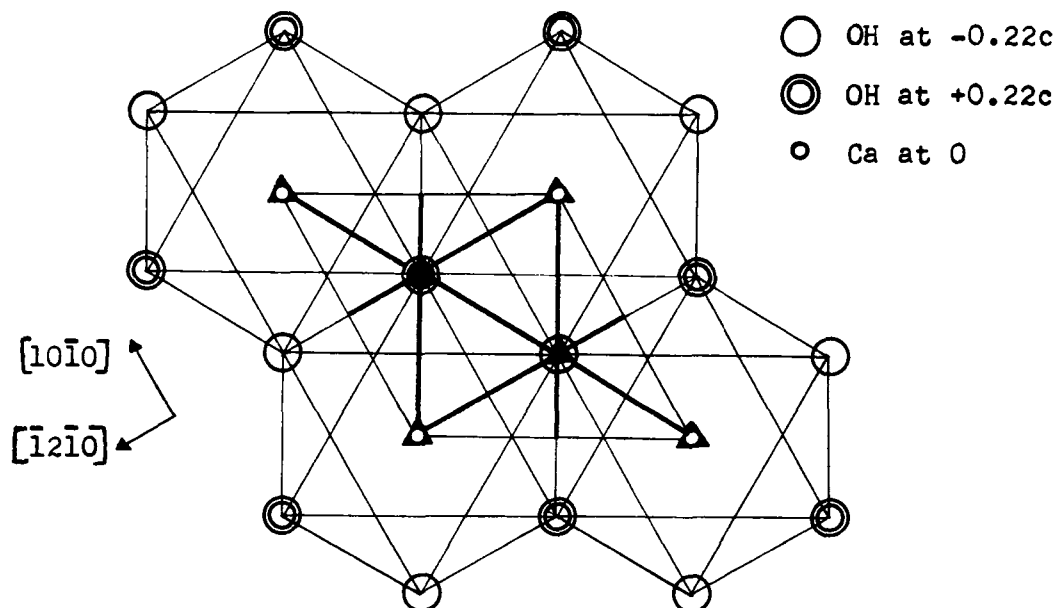


Fig.II.1. Structure of  $\text{Ca}(\text{OH})_2$  projected on  $\{0001\}$  plane. Some elements of the space group,  $D_{3d}^3$ , are shown within the unit cell. These are:  $\text{---}$  - mirror plane,  $\blacktriangle$  - three-fold rotation axis. The calcium atoms are situated at inversion centers.

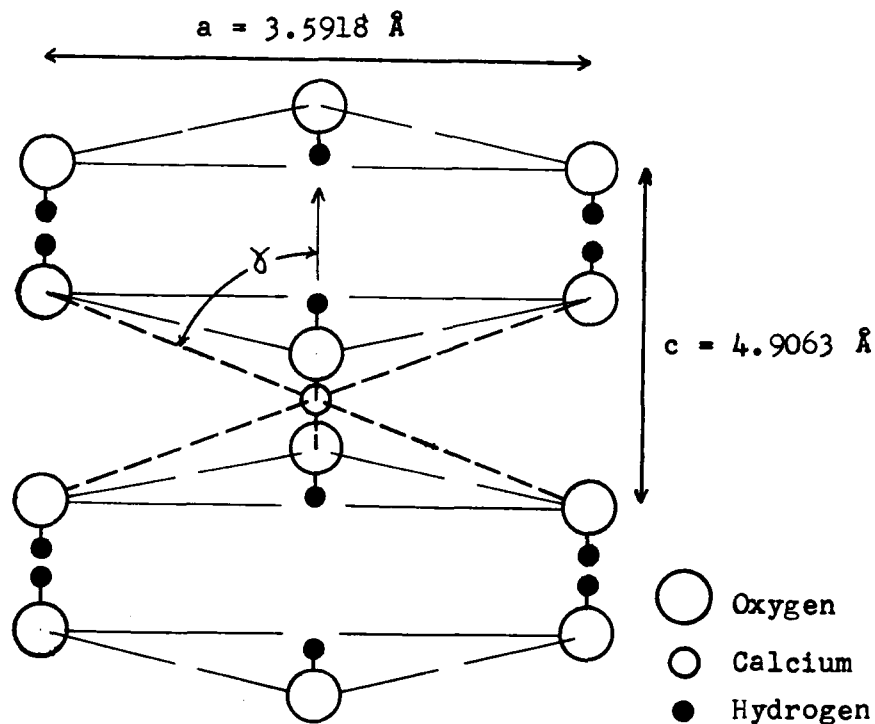


Fig.II.2. Nearest- and next nearest-neighbor environment of calcium atom in  $\text{Ca}(\text{OH})_2$ . Unit cell dimensions at  $T=293^\circ\text{K}$ . are shown. The angle  $\gamma = 61^\circ$  at  $T=293^\circ\text{K}$ . ( $\gamma = 54.7^\circ$  for a cubic octahedron).

TABLE II.I

Structural and other Data for  $\text{Ca}(\text{OH})_2$  Crystal

source	data			
Ref. 2	Linear thermal expansion coefficients			
	$\alpha_a = (0.98 \pm 0.08) \times 10^{-5} \text{ deg}^{-1}$		$\alpha_c = (3.34 \pm 0.20) \times 10^{-5} \text{ deg}^{-1}$	
Ref. 10		T=133°K	T=293°K	
	unit cell parameter 'a'	3.5862 ± 0.0006 Å	3.5918 ± 0.0003 Å	
	unit cell parameter 'c'	4.8801 ± 0.0017 Å	4.9063 ± 0.0007 Å	
	Ca-O distance ( $R_0$ )	2.366 ± 0.001 Å	2.371 ± 0.001 Å	
	structure parameter $z_0$	0.2346 ± 0.0002	0.2341 ± 0.0003	
Unit cell dimensions were taken from Ref. 4, converted from KX to Å units, and corrected for thermal expansion using the coefficients of Megaw (Ref. 2).				
This work.	Effective thermal expansion coefficient for the position parameter $z_0$ , $\alpha_{z_0} = -1.375 \times 10^{-5} \text{ deg}^{-1}$ , was calculated assuming usual exponential temperature dependence. Busing and Levy data (Ref. 10) was used at 133°K and 293°K.			
	Temperature dependence of $R_0$ and $\gamma$ (see Fig. II.2) can be calculated from the following formulae derived from unit cell geometry.			
	$R_0 = (1/3 a^2 + z_0^2 c^2)^{1/2} \quad \gamma = \text{ARCTan}(a/\sqrt{3}z_0c)$			
	Debye Temperature $\theta = 260^\circ\text{K}$ was calculated from low temperature specific heat formula $c_v = 2.64 \times 10^{-5} T^3$ obtained from Ref. 12.			

the calcium atom.

## II. LATTICE DYNAMICS

The two OH groups in the unit cell make possible a highly complex phonon spectrum. Infra-red (IR) and Raman spectroscopy<sup>13</sup> reveal the presence of OH rotatory modes and Ca-OH vibratory modes in addition to the fundamental OH stretching mode. Combinations of these also exist. Inelastic neutron scattering (INS) in the powder<sup>14</sup> and in the crystal<sup>15</sup> has also yielded evidence of some of these modes in addition to an acoustical branch of normal mode. Mitra<sup>16</sup> and Oehler and Gunthard<sup>17</sup> have explained the combinations theoretically.

We present in this section a short summary of results from these optical investigations which will be pertinent to our problem. Specifically, we concentrate on those  $\vec{k} = 0$  optical modes which we expect to be dominant in the  $\text{Mn}^{2+}$  vibronic coupling.

According to factor group analysis, the dispersion surface of  $\text{Ca}(\text{OH})_2$  with 5 atoms per unit cell, has 15 distinct branches, of which 10 correspond to optical lattice modes, 3 to acoustical modes, and 2 to internal OH modes. The physical nature of the <sup>67'</sup>12 optical modes is sketched in Fig. II.3. The first Brillouin zone of  $\text{Ca}(\text{OH})_2$  is shown in Fig. II. 4. The symmetry elements of each little group  $G_k$  being known, it is possible to calculate the characters of the translation group representations using formulae given by Mitra<sup>18</sup> and Oehler and Gunthard<sup>20</sup>. It is customary, however, to list the number of times each of the latter representations is contained in the little group representations, rather

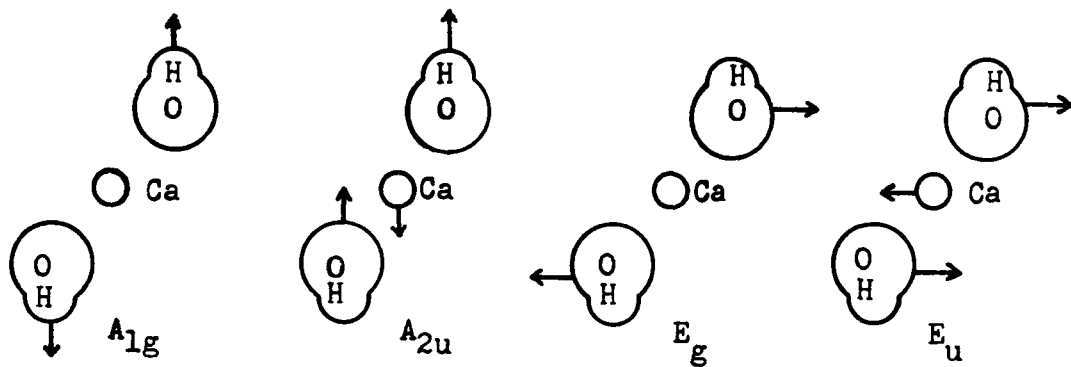


Fig.II.3.  $T_1$  optical modes of vibration of  $\text{Ca}(\text{OH})_2$  crystal for  $k=0$  (from Ref.18).

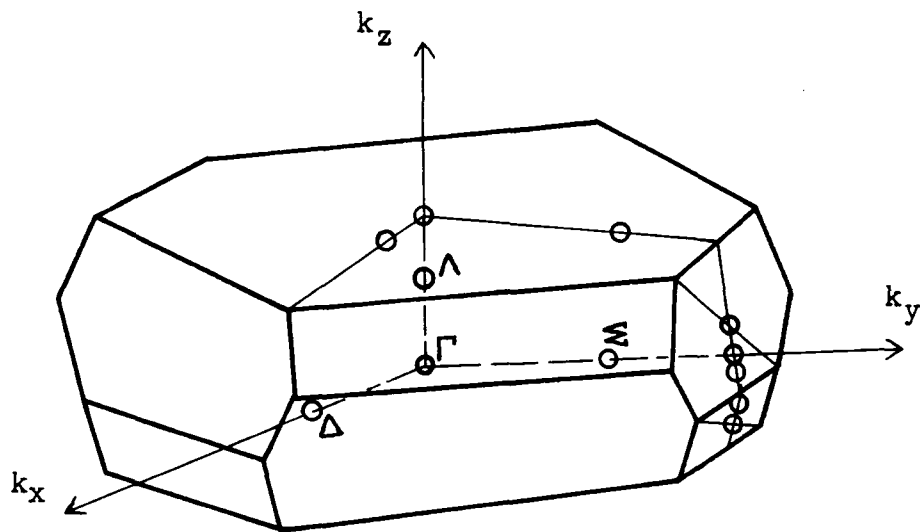


Fig.II.4. The first Brillouin zone of the trigonal lattice ( $r < s/\sqrt{2}$ ) (from Ref.19). The little group at  $\Gamma(0,0,0)$  is  $D_{3d}$ , at  $\Delta(k_x,0,0)$  is  $C_2$ , at  $\Sigma(0,k_y,0)$  is  $C_s$ , and at  $\Lambda(0,0,k_z)$  is  $C_{3v}$ .

than the explicit translation group character table. This gives directly the number of modes of each type. Results of a partial factor group analysis<sup>17</sup> for the little group  $D_{3d}$  is given in Table II. II.

We expect only those modes which involve the relative motion of  $Mn^{2+}(Ga)$  and OH to be responsible for any  $Mn^{2+}$  vibronic coupling. The frequencies of these modes, the so called T'-modes, are listed in Table II. III<sup>17</sup>. This point will be discussed further in Chapter III.

TABLE II.II

Types of Modes (symmetry coordinates) for  $\text{Ca}(\text{OH})_2$  Crystal

little group $G_k$	wave vector $\vec{k}$ of phonon	irred. rep. of $G_k$	modes				
			type				
			$n_i$	T	T'	R'	$n'_i$
$D_{3d}$	$k_x = k_y = k_z = 0$	$A_{1g}$	2	0	1	0	1
		$A_{1u}$	0	0	0	0	0
		$A_{2g}$	0	0	0	0	0
		$A_{2u}$	3	1	1	0	1
		$E_g$	2	0	1	1	0
		$E_u$	3	1	1	1	0

TABLE II.III

Fundamental T' ( $\vec{k}=0$ ) Mode Frequencies

mode type	$\vec{k}=0$ symmetry property	mode frequency $\text{cm}^{-1}$
T'	$A_{1g}$	282
T'	$E_g$	247
T'	$A_{2u}$	321
T'	$E_u$	421

## CHAPTER III

### THEORY

#### I. CRYSTAL FIELD THEORY OF THE $Mn^{2+}$ ION

The ground state of the free  $Mn^{2+}$  ion is  $3d^5 6S_{5/2}$  in Russell-Saunders coupling. The ground state of the ion in a weak crystalline electric field of cubic symmetry is  $(t_{2g})^3(e_g)^2 6A_{1g}$ . Neglecting spin, group theory predicts no splitting of this state in a crystal field since the state is orbitally non-degenerate. Physically, we would expect the 6-fold spin degeneracy to remain, since an electric field cannot affect spins directly. Since we observe EPR only in this ground state, the lack of orbital angular momentum would normally lead us to anticipate no crystalline field interactions. Contrary to expectations, however, the ground state of  $Mn^{2+}$  in a cubic environment, such as that of MgO, splits into one Kramers doublet and one quartet<sup>21</sup>. The ground state of  $Mn^{2+}$  in lower symmetries splits into three Kramers doublets. In addition, there is almost always a large hyperfine structure.

Bethe, in 1929, had showed that by means of the double group the state  $6A_{1g}$  in cubic symmetry decomposes to  $\Gamma_7$  (2-fold) and  $\Gamma_8$  (4-fold) levels<sup>22</sup>. In lower symmetries the  $\Gamma_8$  level splits further into two 2-fold levels. In spite of the fact that crystalline field splittings of the S-state were rigorously predictable by group theory, physical mechanisms responsible for the splittings remained elusive. As we shall see in part IIIA of this chapter, the total crystalline field splitting is, in general, the result of the combined actions of the crystalline potential

( $V_c$ ), spin-orbit coupling ( $W_{LS}$ ), and spin-spin coupling ( $W_{SS}$ ). The splitting is also affected by lattice vibrations which modulate the crystalline electric field. In part IIIB we review S-state hyperfine interactions, and in part IIIC, the theory of the superhyperfine interaction pertinent to this work.

## II. THE HAMILTONIAN FORMALISM AS APPLIED TO $Mn^{2+}$ IN $Ca(OH)_2$

We anticipate that the  $Mn^{2+}$  ion substitutionally replaces the  $Ca^{2+}$  ion in the  $Ca(OH)_2$  lattice. The point symmetry of the  $Mn^{2+}$  ion should therefore be  $D_{3d}$ . A spin-Hamiltonian which is invariant in this symmetry and which accounts for all sources of  $Mn^{2+}$  spin potential energy, is<sup>23</sup>

$$H(s) = \beta \vec{H} \cdot \vec{g} \cdot \vec{S} + \vec{I} \cdot \vec{A} \cdot \vec{S} + 1/3 b_2^0 O_2^0 + 1/60 b_4^0 O_4^0 + 1/60 b_4^3 O_4^3 \quad (III.1)$$

The terms are written in decreasing order of magnitude. The superhyperfine term has been omitted. The first term in Eq. (III.1) is the Zeeman term; the second is the hyperfine term; the remainder are the so-called crystal field terms. The  $O_n^m$  are functions of spin operators and have been listed by Orbach<sup>24</sup>. We assume that the g-tensor, the hyperfine tensor, and the crystal field tensors, all have the same set of principal axes. We further assume that the g-tensor and the A-tensor have axial symmetry with principal values,  $g_{11}$ ,  $g_{\perp}$ , and A and B respectively.

In order to diagonalize the Zeeman term, and thus simplify the calculation of matrix elements of Eq. (III.1), we transform to a coordinate system whose z axis, oriented at  $(\beta, \alpha)$  relative to the crystal field axes, is the quantization axis of the electron spin. Transformation

formulae for  $0_2^0$ ,  $0_4^0$ , and  $0_4^3$  have been given by Vinokurov et. al.<sup>23</sup> and by Thyer et. al.<sup>25</sup>. The eigenvalues of Eq. (III.1) to second order perturbation in crystal field terms and hyperfine terms (including cross terms) are

$$E_{Mm} = g\beta HM + d_2^0 + d_4^0 + KMm + \frac{1}{g\beta H_0} \left\{ \sum_{m=1}^n \frac{|d_n^{m-}|^2 - |d_n^{m+}|^2}{m} + R \right. \\ \left. + R_x m \left( \frac{B^2 - A^2}{2K} \right) \sin 2\beta + \frac{M[I(I+1) - m^2]}{4} \left( \frac{A^2 B^2}{k^2} + B^2 \right) \right. \\ \left. + \frac{Mm^2}{2} \left( \frac{B^2 - A^2}{2K} \right)^2 \sin^2 2\beta - \frac{AB^2 m}{2k} [s(s+1) - M^2] \right\},$$

where  $d_n^{m\pm} = \gamma a_n^{m\pm} \langle M | O_n^m | M \pm m \rangle$  for  $n = 2, m = 0, 1, 2; \gamma = 1/3$   
 $n = 4, m = 0, 1, 2, 3; \gamma = 1/60,$

$$R = d_2^{1-} (d_4^{1-})^* - d_2^{1+} (d_4^{1+})^* + d_4^{1-} (d_2^{1-})^* - d_4^{1+} (d_2^{1+})^* \\ + 1/2 d_2^{2-} (d_4^{2-})^* - 1/2 d_2^{2+} (d_4^{2+})^* + 1/2 d_4^{2-} (d_2^{2-})^* \\ - 1/2 (d_2^{2+})^* d_4^{2+},$$

$$R_x = d_2^{1-} d_x^+ + d_4^{1-} d_x^+ + d_x^- (d_2^{1-})^* + d_x^- (d_4^{1-})^* - d_2^{1+} d_x^- - d_x^+ d_4^{1+} \\ - d_x^+ (d_2^{1+})^* - d_x^+ (d_4^{1+})^*; \quad (III.2)$$

$$d_x^+ = \langle M | S_x | M \pm 1 \rangle.$$

The  $a_n^{m\pm}$  have been listed by Vinokurov et al.<sup>23</sup>. The elements  $\langle M | O_n^m | M \pm 1 \rangle$  have been extensively tabulated by Buckmaster<sup>26</sup> and Hutchings<sup>27</sup>. From Eq.(III.2) we obtain the values of magnetic field at which resonances occur for constant frequency.

$$\begin{aligned}
H\left(\pm \frac{5}{2}, m \rightleftharpoons \pm \frac{3}{2}, m\right) &= H_0 \mp 4a_2^0 \mp 4a_4^0 - \frac{1}{H_0} \left\{ \frac{8}{9} |a_2^1|^2 - \frac{4}{9} |a_2^2|^2 \right. \\
&- \frac{1}{40} |a_4^1|^2 + \frac{1}{20} |a_4^2|^2 + \frac{1}{120} |a_4^3|^2 + \frac{1}{2} a_2^1 (a_4^{1-} + a_4^{1+}) \\
&+ \frac{1}{2} a_2^2 (a_4^{2-} + a_4^{2+}) \mp [2a_2^1 + (a_4^{1-} + a_4^{1+})] m \left( \frac{B^2 - A^2}{2k} \right) \sin 2\beta \\
&\left. + \frac{1}{4} \left( \frac{35}{4} - m^2 \right) \left( \frac{A^2 B^2}{k^2} + B^2 \right) + \frac{1}{2} m^2 \left( \frac{B^2 - A^2}{2k} \right)^2 \sin^2 2\beta + 2m \frac{AB^2}{k} \right\} - mK.
\end{aligned}$$

$$\begin{aligned}
H\left(\pm \frac{3}{2}, m \rightleftharpoons \pm \frac{1}{2}, m\right) &= H_0 \mp 2a_2^0 \pm 5a_4^0 - \frac{1}{H_0} \left\{ -\frac{1}{9} |a_2^1|^2 + \frac{5}{9} |a_2^2|^2 \right. \\
&+ \frac{1}{5} |a_4^1|^2 + \frac{9}{80} |a_4^2|^2 - \frac{1}{120} |a_4^3|^2 + \frac{1}{20} |a_4^4|^2 - \frac{1}{2} a_2^1 (a_4^{1+} + a_4^{1-}) \\
&+ \frac{1}{4} a_2^2 (a_4^{2+} + a_4^{2-}) \mp [a_2^1 - \frac{5}{4} (a_4^{1-} + a_4^{1+})] m \left( \frac{B^2 - A^2}{2k} \right) \sin 2\beta + \frac{1}{4} \left( \frac{35}{4} - m^2 \right) \\
&\left. \left( \frac{A^2 B^2}{k^2} + B^2 \right) + \frac{1}{2} m^2 \left( \frac{B^2 - A^2}{2k} \right)^2 \sin^2 2\beta + m \frac{AB^2}{k} \right\} - mK.
\end{aligned}$$

$$\begin{aligned}
H\left(\frac{1}{2}, m \rightarrow -\frac{1}{2}, m\right) &= H_0 - \frac{1}{H_0} \left\{ -\frac{4}{9} |a_2^1|^2 + \frac{8}{9} |a_2^2|^2 - \frac{1}{4} |a_4^1|^2 - \frac{1}{10} |a_4^2|^2 \right. \\
&+ \frac{1}{60} |a_4^3|^2 + \frac{1}{3} a_2^1 (a_4^{1+} + a_4^{1-}) - a_2^2 (a_4^{2+} + a_4^{2-}) + \frac{1}{4} \left( \frac{35}{4} - m^2 \right) \left( \frac{A^2 B^2}{k^2} + B^2 \right) \\
&\left. + \frac{1}{2} m^2 \left( \frac{B^2 - A^2}{2k} \right)^2 \sin^2 2\beta \right\} - mK. \tag{III.3}
\end{aligned}$$

Eq. (III.1) is identical to that used by Bleaney and Trenam

$$(1954)^{28} \text{ for } b_2^0 = D, \quad b_4^0 = \frac{1}{3}(F-a), \quad b_4^3 = \frac{20\sqrt{3}}{3} a. \tag{III.4}$$

### III. CALCULATION OF SPIN-HAMILTONIAN PARAMETERS

#### A. Crystal Field Parameters and g-values

##### (i) Static Splittings: The Point-Multipole (PM) Model

Calculations of the crystal field parameters and the g-values pertaining to  $d^5$  ions in  $^6S$  ground states involve the Zeeman interaction ( $W_H$ ),  $V_C$ ,  $W_{LS}$ , and  $W_{SS}$ . Various combinations of these interactions have been used in perturbation calculations up to as high as the sixth-order. The reasons such high order perturbations are needed are four-fold.

(1) Matrix elements of any even-order  $V_C$  and matrix elements of  $W_{LS}$  within any electrostatic term individually vanish<sup>29</sup> so that  $V_C$  and  $W_{LS}$  cannot cause splitting in the first order. (2)  $V_C$  cannot, by itself, cause ground state splitting in any order of perturbation since the  $^6S$  ground state is the only state with spin multiplicity 6, and in the non-relativistic approximation, matrix elements of  $V_C$  vanish between terms with different spin multiplicities. (3)  $W_{LS}$  acting alone only shifts the ground state since it couples the ground state to only one other state, the  $^4P$ <sup>30</sup>. (4)  $W_{SS}$  acting alone only shifts the ground state since it couples the ground state to only one other state, the  $4D$ <sup>31</sup>.

If configurations other than  $d^5$  are included, perturbations of lower order are possible. Pryce<sup>32</sup> was the first to study the influence of  $V_C$  and  $W_{SS}$  via the  $^6D$  term of the higher-lying configuration  $3d^44s$ . In recent reviews, Sharma, Das, and Orbach<sup>33,34</sup> (hereafter described as SDO) have extended the number of possible D-mechanisms (SDO used the 'D' notation, as used by Bleaney and Trenam<sup>28</sup>, instead of the  $b_2^0$  notation

used in this work (see Eq. III.4). They have described these mechanisms collectively as point multipole (PM) mechanisms since they are based on the assumption that the lattice is wholly ionic. Since  $\text{Ca}(\text{OH})_2$  is highly ionic we shall not attempt to apply mechanisms based on covalency<sup>38</sup>.

The SDO D-mechanisms,  $D_{\text{BO}}$ ,  $D_{\text{SS}}$ ,  $D_{\text{ODS}}$ , and  $D_{\text{WC}}$ <sup>33</sup> are listed in Table III.I. The values of these quantities at room temperature (RT) were calculated using the formulae given by SDO. Excepting  $D_{\text{BO}}$ , these formulae contain  $B_2^0$ , the coefficient of the axial potential, so that the application of these formulae to this problem involved the calculation of  $B_2^0$  for the  $[\text{Ca}(\text{OH})_6]^{4-}$  complex. The point-charge lattice summation method was employed to compute  $B_2^0$  since the structure of this complex is simple.

The result is:

$$\begin{aligned} D &= D_{\text{SS}} + D_{\text{ODS}} + D_{\text{WC}} \\ &= -0.07305B_2^0 + 2.1044(B_2^0)^2 - 1.7417(B_2^0)^2. \end{aligned} \quad (\text{III.5})$$

$B_2^0$  for  $D_{3d}$  symmetry is:

$$B_2^0 = \frac{-6e(3\cos^2\gamma-1)}{R^3} \quad (\text{III.6})$$

where  $R$  is the anion-cation distance, in units of the Bohr radius, and  $e$  is the electronic charge on the cation.  $\gamma$  is the angle between the  $c$  axis and the anion-cation bond direction.

Included in Table III.I is  $D_{\text{VH}}$ , the value of  $D$  calculated by van Heuvelen<sup>35</sup>. By using relativistic Hartree-Fock wavefunctions for the basis states it can be shown that matrix elements of  $V_c$  no longer vanish between terms with different spin multiplicities. Although it has the

TABLE III.I

 ${}^6S$ -state Splitting Mechanisms Within The PM Model

Source	Parameter	General mechanism type	Predicted inverse power of $R_0$	RT value* $\times 10^4 \text{cm}^{-1}$
Ref. 33,34	$D_{BO}$	${}^6S - T_{IG} \begin{pmatrix} 4 & 4 & 4 & 4 \\ P & F & G & G \end{pmatrix} - V_4 \begin{pmatrix} 4 & 4 & 4 & 4 \\ P & F & G & G \end{pmatrix} - W_{LS} \begin{pmatrix} 4 & 4 & 4 & 4 \\ P & F & G & G \end{pmatrix}$	5	0**
Ref. 33,34	$D_{SS}$	d-s, d-d and d-g admixtures by $W_{SS}$	3	-14.3
Ref. 33,34	$D_{ODS}$	$3d \begin{matrix} 56 \\ W_{LS} \end{matrix} S - (\text{other}) \begin{matrix} 4 \\ W_{LS} \end{matrix} T_{IG} \left[ \begin{pmatrix} 4 & 4 & 4 & 4 \\ P & F & G & P \end{pmatrix} \begin{pmatrix} 4 & 4 & 4 & 4 \\ G & P & F & F \end{pmatrix} \right] - 3d \begin{matrix} 56 \\ W_{LS} \end{matrix} S$	6	+8.1
Ref. 33,34	$D_{WC}$	(All $3d^5$ ) $\begin{matrix} 6 \\ W_{LS} \end{matrix} S - \begin{matrix} 4 \\ W_{LS} \end{matrix} D - \begin{matrix} 4 \\ W_{LS} \end{matrix} P - \begin{matrix} 6 \\ W_{LS} \end{matrix} S$	6	-6.7
Ref. 35	$D_{VH}$	(Relativistic within $3d^5$ ) $\begin{matrix} 6 \\ W_{LS} \end{matrix} S - \begin{matrix} 4 \\ W_{LS} \end{matrix} P - \begin{matrix} 6 \\ W_{LS} \end{matrix} S$	3	-90.0
Ref. 39	$a_W$	12 different mechanisms involving $W_{LS}, V_c, W_{SS}$ , to 4th-, 5th-, and 6th-orders, including spin doublets	10	+0.6
Ref. 39	$\epsilon_W$	(All $3d^5$ ) $\begin{matrix} 6 \\ W_{LS} \end{matrix} S - \begin{matrix} 4 \\ W_{LS} \end{matrix} P - \begin{matrix} 6 \\ W_{LS} \end{matrix} S$ ; $\begin{matrix} 6 \\ W_{LS} \end{matrix} S - \begin{matrix} 4 \\ W_{LS} \end{matrix} P - \begin{matrix} 6 \\ W_{LS} \end{matrix} S$	$\Delta g = 2.0019$	$\Delta g = -0.0004$

Source	Parameter	General Mechanism type	Predicted inverse power of $R_0$	RT value $\times 10^4 \text{ cm}^{-1}$
Ref. 40	$a_p$	$W_{LS}$ and $W_{SS}$ to 6th-order in strong field approx.	even or odd $\sim 10$	$\sim +15$
Ref. 41	$a_G$	Diag. of $3d^5$ secular det.	" "	$\sim +10$
Ref. 42	$a_L$	Diagonalization neglecting $W_{SS}$	" "	$\sim +10$

\* Implicit in these calculations are physical quantities, such as the crystal field parameter  $Dq$ , spin-orbit coupling constant  $\zeta$ , Racah Parameters B and C, etc., assumed by the authors. The values of these quantities which were assumed vary slightly from reference to reference. Values quoted for  $D_{VH}$ ,  $a_W$ ,  $\epsilon_W$ ,  $a_p$ ,  $a_G$ , and  $A_L$  were taken directly from the references.

\*\*  $D_{BO}$  was computed from the formula given by SDO using the point-charge lattice summation method.

same sign and comparable magnitude as our experimental  $D$ , we shall ignore  $D_{\text{VH}}$  in our further discussion.

Since we anticipate  $b_4^0$  to be determined by 'a' to a good approximation, the table also includes contributions to 'a' coming from several possible mechanisms. It is impossible to calculate accurately the values of  $a_{\text{P}}$ ,  $a_{\text{G}}$ , or  $a_{\text{L}}$  for the  $\text{Ca}(\text{OH})_2:\text{Mn}^{2+}$  system since the separations in energy between the electrostatic terms are unknown.

(ii) Dynamic Splittings: Effects of Lattice Vibrations (phonons)

We have seen in the previous section of this chapter that the crystal field parameters are functions of crystalline potentials of various symmetries. Since these potentials are linear combinations of spherical harmonics they involve the position coordinates of the source charges to various powers. When these coordinates are thermally modulated, the observed value of a parameter,  $G$ , is a time average,  $\langle G \rangle_t$ , which depends not only on the average value of the source coordinates (a change in this average value constitutes thermal expansion) but also on the detailed character of the vibrations. For example, for the simple case of harmonic modulation of the anion-cation distance,  $d(t) = d_0(1 + \epsilon \cos \omega t)$ , the time average value of  $d^n$  is  $\langle d^n \rangle = d_0^n [1 + n(n+1) \epsilon^2/4]$ ,  $n \geq 0$ . This means that a purely harmonic vibration of this type ( $A_{1g}$ ), while not affecting thermal expansion at all, does change the average value of the crystalline potential and thus also  $\langle G \rangle_t$ <sup>43</sup>. Since the paramagnetic ion is subject to lattice vibrations the Hamiltonian (such as Eq. (III.1)) must be considered a 'dynamical' one which reflects the average site symmetry. Each

coefficient of this dynamical Hamiltonian is the average of a distribution which has been motionally narrowed and is not, in general, equal to the corresponding parameter in the static Hamiltonian<sup>37</sup>. This notion of averaging a motionally narrowed distribution has been employed in describing the effect of lattice vibrations on optical spectra and on the chemical shift. The result is that the position of the spectral line depends explicitly on the temperature through its dependence on the mean-square amplitude of the lattice vibrations<sup>37</sup>.

Assuming that the substitution of an  $\text{Mn}^{2+}$  ion for a lattice cation does not disturb the normal modes or set up local modes, it can be shown that the functional form of the temperature dependence of some EPR Hamiltonian parameters is quite similar to that for, say, optical linewidths<sup>44</sup>, and the chemical shift. There are two approaches. The most fundamental approach would be to calculate the normal modes of the  $[\text{Ca}(\text{OH})_6]^{4-}$  system in a manner similar to Van Vleck's calculations in the alums when treating the Jahn-Teller effect<sup>45</sup> and spin-lattice relaxation<sup>46</sup>. Two important points in this calculation for the alums were the following (1) Paramagnetic ions were subject to crystalline fields of predominantly cubic symmetry but with a small trigonal component. (2) The symmetry of the normal modes was  $O_h$ . Although (1) holds true for the  $\text{Ca}(\text{OH})_2:\text{Mn}^{2+}$  system, (2) does not, since the normal modes in this crystal for  $\vec{k} = 0$  possess  $D_{3d}$  symmetry. (See Table II.II)

The 'vibronic' interaction, i.e., the interaction between the lattice modes and orbits of the  $\text{Mn}^{2+}$  electrons is given by the so-called orbit-lattice interaction

$$W_{OL} = \sum_{i,j} V_j(\Gamma_{ig}) \epsilon(\Gamma_{ig}j) \quad (\text{III.7})$$

The  $\epsilon(\Gamma_{ig}j)$  are the normal coordinates (displacement operators) of the  $[\text{Ca}(\text{OH})_6]^{4-}$  system which are, in turn, those linear combinations of components of the strain tensor which transform as the  $j$ th subvector of the representation  $\Gamma_{ig}$ . If Eq. (III.7) is assumed to operate only within  $d^5$ , even vibrations need only be considered. We shall assume the  $\Gamma_{ig}$  to be those characterizing  $T'$  modes only. The  $\Gamma_{ig}$  are, of course, those  $T'$  representations which are permitted under one of the little groups of the space group  $D_{3d}^3$ . The  $V_j(\Gamma_{ig})$  are linear combinations of spherical harmonics (electronic operators) which transform as the  $\Gamma_{ig}$ . The components of the strain tensor are the normal coordinates  $q_{lm}$  associated with the lattice heat waves. These quantities introduce the temperature dependence, ie.

$$\epsilon(\Gamma_{ig},j) = \sum_{m=1}^3 \sum_{\lambda=1}^N a_{j\lambda} q_{\lambda m} \quad (\text{III.8})$$

where  $m$  denotes the phonon polarization, and  $N$  the total number of atoms in the crystal. The phonon operator is defined in the particle number representation by

$$\langle n_{\lambda m} | q_{\lambda m} | n_{\lambda m} + 1 \rangle = \langle n_{\lambda m} + 1 | q_{\lambda m} | n_{\lambda m} \rangle = [h(n_{\lambda m} + 1)/2\pi M v_{\lambda m}]^{1/2} \quad (\text{III.9})$$

where  $\langle n_{\lambda m} \rangle = (1 - e^{-h\nu_{\lambda m}/kT})^{-1}$  and  $M$  is the mass of the crystal.

We terminate the discussion of the first approach by outlining the required calculations. We shall not attempt such calculations. To first order  $W_{OL}$  simply shifts the energy of the  $S$  ground state. Therefore,

one would naturally attempt to use  $W_{OL}$  as yet another perturbation term in a comprehensive treatment like that of Sharma, Das, and Orbach<sup>33,34</sup> (see Table III.I). It can be seen from this table that  $W_{OL}$ , used in combination with  $W_{LS}$  and  $V_c$ , will affect  $D_{BO}$  and  $D_{WC}$  via the  $\vec{k} = 0$  T' modes transforming as  $A_{1g}$  and  $E_g$  and will affect  $D_{ODS}$  via the  $\vec{k} = 0$  T' modes transforming as  $A_{2u}$  and  $E_u$ . It is unlikely that a Waller-like mechanism will affect  $D_{SS}$  to any great extent since its effect in spin-lattice relaxation is very small<sup>46</sup>. Calculations such as these have not yet appeared in the literature. Their importance should be recognized mostly in non cubic crystals since experimentally it is known that the temperature dependence of 'a' is determined mainly by thermal expansion<sup>37</sup>. We shall discuss the use of  $W_{OL}$  in more detail in the next section devoted to hyperfine structure.

The second approach, and the one we shall use for describing the temperature dependence of the crystal field parameters in this experiment, has been discussed by Bloembergen<sup>37</sup>. We expand the parameter of interest,  $G(\vec{r}_i - \vec{r}_0)$ , in terms of the deviations  $\vec{\delta}_i = \vec{r}_i - \vec{r}_0$  of the magnetic ion's Z effective neighbours located at  $\vec{r}_i$  ( $i=1,2,\dots,Z$ ) from their equilibrium positions  $\vec{\Delta}_i = \vec{r}_i - \vec{r}_0$  relative to the ion at  $\vec{r}_0$ . We assume that G is a scalar. To second order in the local coordinate deviations

$$G(\vec{\Delta}_i) = G_0 + \sum_{i=1}^Z \left( \frac{\partial G}{\partial \Delta_i} \right)_0 \cdot \vec{\delta}_i + \frac{1}{2} \sum_{i,j=1}^Z \vec{\delta}_i \cdot \left( \frac{\partial^2 G}{\partial \Delta_i \partial \Delta_j} \right) \cdot \vec{\delta}_j \quad (\text{III.10})$$

Lattice vibrations are introduced by expanding the  $\vec{\delta}_i$  in terms of the normal coordinates  $\vec{\xi}_\lambda$

$$\vec{\delta}_i = \sum_{\lambda} C_{i\lambda} \vec{\xi}_{\lambda} \quad (\text{III.11})$$

where 
$$\vec{\xi}_{\lambda} = \hat{\lambda} \xi_{\lambda 0} \cos[\omega_{\lambda} t - \vec{k}_{\lambda} \cdot \vec{r} + \alpha_{\lambda}(t)] \quad (\text{III.12})$$

Eq.(III.12) defined a travelling wave of amplitude  $\xi_{\lambda 0}$ , angular frequency  $\omega_{\lambda}$ , wave vector  $\vec{k}_{\lambda}$ , time dependent phase  $\alpha_{\lambda}$  (due to finite phonon lifetimes) and unit polarization vector  $\hat{\lambda}$ . Since the  $\vec{\delta}_i$  are local coordinate changes the coefficients  $C_{i\lambda}$  weigh optical modes (specifically T' modes) most heavily. Substituting Eq. (III.11) and Eq. (III.12) into Eq. (III.10) and averaging over times long compared to phonon lifetimes (thus allowing the phases  $\alpha_{\lambda}$  to fluctuate randomly) we obtain:

$$\langle G \rangle_t = G_0 + \frac{1}{4} \sum_{i,j=1}^Z \sum_{\lambda} \hat{\lambda} \cdot \left( \frac{\partial^2 G}{\partial \Delta_i \partial \Delta_j} \right) \cdot \hat{\lambda} C_{i\lambda} C_{j\lambda} \xi_{\lambda 0}^2. \quad (\text{III.13})$$

This may be written in the simpler form

$$\langle G \rangle_t = G_0 + \frac{1}{4} \sum_{\lambda} \left( \frac{\partial^2 G}{\partial \xi_{\lambda}^2} \right)_0 \xi_{\lambda 0}^2. \quad (\text{III.14})$$

Equating the energy of a lattice vibration to that of a quantum-mechanical harmonic oscillator leads to

$$\begin{aligned} \xi_{\lambda 0}^2 &= \frac{2\hbar}{\omega_{\lambda}} \left( \frac{1}{2} + \frac{1}{e^{\hbar\omega_{\lambda}/kT} - 1} \right) \\ &= \frac{\hbar}{\omega_{\lambda}} \text{COTH} \left( \frac{\hbar\omega_{\lambda}}{2kT} \right), \end{aligned} \quad (\text{III.15})$$

so that Eq. (III.14) becomes

$$\langle G \rangle_t = G_0 + \frac{\hbar}{4} \sum_{\lambda} \left( \frac{\partial^2 G}{\partial \xi_{\lambda}^2} \right)_0 \frac{1}{\omega_{\lambda}} \text{COTH} \left( \frac{\hbar\omega_{\lambda}}{2kT} \right). \quad (\text{III.16})$$

We let the  $\lambda$  run over the T' optical modes. Using the frequencies given in Table II.III, and noting the degeneracies of the modes, Eq. (III.16) becomes, in the case when  $G = D$ ,

$$\langle D \rangle_t = D_0 + 4.97 \times 10^{-42} K_1 \coth\left(\frac{196}{T}\right) + 11.3 \times 10^{-42} K_2 \times \coth\left(\frac{172}{T}\right), \quad (\text{III.17})$$

neglecting  $W_{OL}$  perturbations via configurational interactions. The  $K_\lambda$ 's are the quantities  $\left(\frac{\partial^2 D}{\partial \xi_\lambda^2}\right)_0$ .  $\lambda$  runs over the  $A_{1g}(T')$  and  $E_g(T')$  modes respectively. Thus by fitting Eq.(III.17) to the experimental curve we shall be able to determine  $D_0$  (the true 'static' D-value, the value of D in the absence of even zero-point vibrations) and the  $K_\lambda$ 's.

## B. Hyperfine Structure (HFS) Parameters A and B

### (i) Static Splittings: Core Polarization

The HFS coupling constant A is a tensor which is the sum of the isotropic Fermi contact tensor and the traceless dipolar tensor. The large HFS which is usually observed for  $Mn^{2+}$  has been explained as follows. Originally, Abragam and Pryce<sup>47</sup> proposed a second order electrostatic interaction between 3d electrons and s-electrons of higher-lying configurations. Detailed work, however, has revealed that this mechanism gives HFS an order of magnitude too small. Heine<sup>48</sup> proposed that it was possible for the 2s and 3s core electrons to become slightly unpaired because of their exchange interaction with the 3d electrons. When the  $Mn^{2+}$  ion is in the  $^6S$  ground state, the spins of the five 3d electrons are oriented parallel( $\uparrow\uparrow\uparrow\uparrow\uparrow$ ). Only those s-electrons which have like spin orientations

are affected by exchange. Consequently, the  $2s(\uparrow)$  and  $3s(\uparrow)$  electrons are attracted outward toward the 3d electrons by exchange forces leaving the  $2s(\downarrow)$  and  $3s(\downarrow)$  electrons to take part in the contact interaction. This effect is called core polarization<sup>49</sup>. Calculations of A based on core polarization will not be carried out. We shall attempt to explain only A as a function of T.

(ii) Dynamic Splittings: The Orbit-Lattice Interaction

Simanek and Orbach<sup>50</sup> have satisfactorily explained the temperature dependence of A of  $Mn^{2+}$  in cubic crystals such as MgO. They proposed that, in addition to core polarization which is by far the dominant mechanism and which is temperature independent,  $W_{OL}$  admixes excited configurations of the form  $3d^4ns$  into the ground  $3d^5$  configuration. In first order,  $W_{OL}$  couples admixed s-states which have spins parallel to the spin of the 3d ground state so that the core polarization is slightly reduced. Important points in the Simanek-Orbach theory are:

- (1) Since  $W_{OL}$  is assumed to operate between configurations involving d and s electrons, only  $j = 2$  terms of Eq.(III.7) are important.
- (2)  $W_{OL}$  is taken as a perturbation to first order only.
- (3) The mean square strains  $\langle \epsilon^2 \rangle$  are obtained from Eq. (III.8) assuming cubic symmetry.

We quote their result.

$$A(T) = A(0) \left[ 1 - CT^4 \int_0^{\theta/T} \frac{x^3 dx}{e^x - 1} \right] \quad (III.18)$$

where C is a constant and  $\theta$  is the average Debye Temperature.

The HFS tensor of  $Mn^{2+}$  in non-cubic crystals is usually slightly anisotropic due to the effect of the dipolar interaction. Since the dipolar tensor is traceless, the contribution of the isotropic Fermi contact interaction is  $(A_{xx} + A_{yy} + A_{zz})/3$ . The  $A_{jj}$  are the HFS coupling constants which are obtained experimentally for magnetic field parallel to the x, y and z direction. For crystals with axial symmetry, this becomes

$$\frac{A+2B}{3}$$

Thus Eq. (III.18) should explain the temperature dependence of this quantity for the  $Ca(OH)_2:Mn^{2+}$  system.

### C. Superhyperfine Structure (SHFS) Parameters

SHFS is accounted for by adding to the spin-Hamiltonian of Eq.(III.1) the additional term

$$H = \sum_N \vec{I}^N \cdot \vec{A}^N \cdot \vec{S} \quad (III.19)$$

where  $\vec{S}$  is the resultant  $Mn^{2+}$  electron spin and  $\vec{I}$  is the proton spin.

The summation is over the neighbouring protons, i.e., 6 in number if we consider only the nearest neighbours of the  $Mn^{2+}$  (see Fig. II.2). The interaction is magnetic and proceeds via chemical bonding. The type of bonding determines the angular properties of Eq.(III.19). The proton HFS tensor  $\vec{A}^N$  may be separated into contact and dipolar parts so that eigenvalues of Eq. (III.19) may be written

$$H = A_s \sum_N \vec{I}_Z^N + A_p \sum_N \vec{I}_Z^N (3 \cos^2 \theta_\zeta - 1) \quad p = \sigma, \pi \quad (III.20)$$

$\theta_\zeta$  is the angle between the external magnetic field and the p-bond axis.

223859

For an arbitrary direction of magnetic field ( $\vec{H}$ ) through the  $[\text{Ca}(\text{OH})_6]^{4-}$  complex, we should expect to see  $3^3=27$  lines if  $A_p \neq 0$ <sup>51</sup>.

For the special case of  $\vec{H} \parallel c$  axis, we should expect 7 equally spaced lines with intensity ratios 1:6:15:20:15:6:1. This should also hold for an arbitrary direction of  $\vec{H}$  if  $A_p = 0$ . We shall attempt only simple computations of  $A_s$  and  $A_p$  from the experimental data. No theoretical analysis will be given.

## CHAPTER IV

### INSTRUMENTATION AND CRYSTAL PREPARATION

The variable temperature work was done using a spectrometer of the straight-detection type operated in the x-band<sup>52</sup>.

A crystal rotating mechanism developed earlier in this laboratory was employed for anisotropy studies at RT<sup>53</sup>. This mechanism enabled the crystal to be rotated about a horizontal axis. Any arbitrary orientation of the crystal relative to the external magnetic field could thus be attained by coupling this mode of rotation with that of the magnet about a vertical axis. A plastic cavity with the inner surface sputtered with gold was used in the LN<sub>2</sub>-RT work. The high temperature cavity (RT-800°K) was of stainless steel, the inner surface being gold electroplated onto copper. Both cavities, whose loaded Qs were about 6000 and 4000, respectively, were operated in the TE<sub>011</sub> mode. They are illustrated in Fig. IV. 1.

Copper-constantan and platinum + 10% Rhodium vs. platinum thermocouples were used for measuring temperatures. Reference temperatures were LN<sub>2</sub> and RT, respectively; the latter was monitored continually to ensure accuracy. Since no special attempts were made to calibrate the thermocouples, accuracy is expected to be of the order of  $\pm 2^{\circ}\text{K}$ . Also, no attempt was made to control temperature. The LN<sub>2</sub> temperature cavity was heated to RT with 3-4 amps. of heater current at 6 volts delivered by a small regulated DC supply. The current was adjusted to an arbitrary value and measurements were made when the temperature was steady. At constant

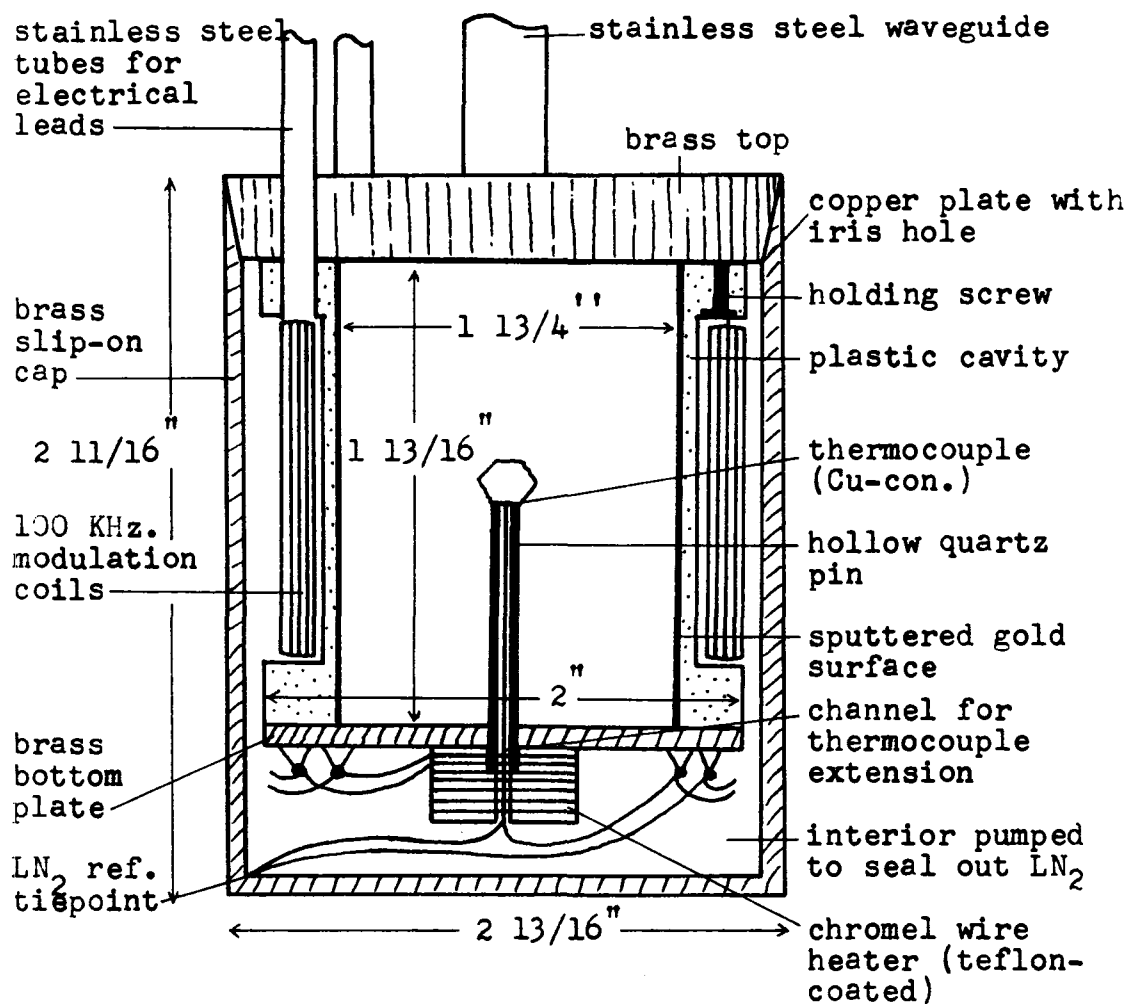


Fig.IV.1a. LN<sub>2</sub>-RT variable temperature cavity.

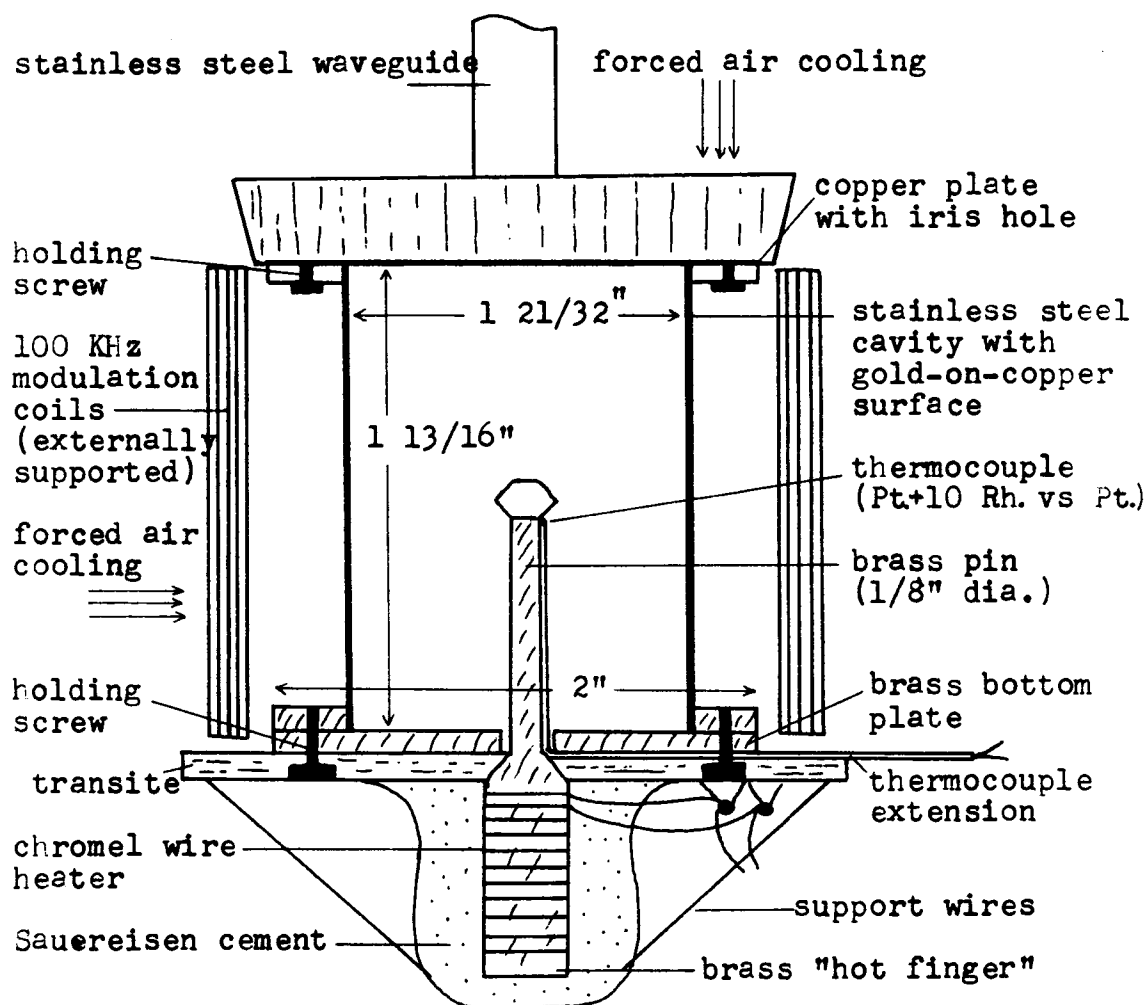


Fig.IV.lb. RT-800°K. variable temperature cavity.

magnetic field modulation levels, temperature stability of about  $\pm 1^{\circ}\text{K}$  was realized after one hr. The high temperature heater was supplied with about 7-8 amps DC at 12 volts maximum. Temperature stability of  $\pm 2^{\circ}\text{K}$ . was obtained with the high temperature cavity within 1 1/2 hr. Forced air cooling of the high temperature cavity kept the change in the cavity resonant frequency to about 25MHz, over its range of operation.

The magnet used was a 15 in. Varian equipped with Fieldial regulation. All field measurements were made with the full 6 in. gap. The large gap was required in order to make room for a large glass dewar which contained the  $\text{LN}_2$  coolant for the low temperature cavity. When the high temperature cavity was employed the large gap also made elaborate external cooling for protection of the polefaces unnecessary. Unfortunately, this arrangement introduced problems with inhomogeneity. To correct partially for inhomogeneity, two proton MR magnetometers were used to plot the magnetic field at the center of the magnet gap as a function of the magnetic field at the poleface center. The oscillator coil of one magnetometer was held temporarily at the center of the magnet gap (with the cavity removed) while the oscillator coil of the other was placed at the center of one of the polefaces. The outputs of both magnetometers were fed through an electronic switch and superimposed on an oscilloscope screen. The frequency measurements for a number of Fieldial settings throughout the range of interest are given in Appendix A. The data show that the frequency relation obtained,  $\text{freq. at gap center (KHz)} = 0.99266 \times \text{freq. at poleface (KHz)} + 0.0036$ , ensured an accuracy of at least  $\pm 0.5 \text{ KHz. (0.1G)}$  in extrapolating the proton MR frequency (field) at the

magnet gap center from the value measured at the center of the poleface. The sample was kept at least to within 1/4 in. of the magnet gap center at all times. As it was, inhomogeneity of the magnetic field over the sample volume ( $\sim 60\text{mm}^3$ ) was estimated to be about 50-100 mG.

The magnetic field was modulated at 100 KHz. by means of small coils placed next to the cavities (see Fig. IV. 1). Very little modulation power was needed with the  $\text{LN}_2$  temperature cavity. On the other hand, about 25 watts of power was required to penetrate the stainless steel of the high temperature cavity.

Single crystals of  $\text{Ca}(\text{OH})_2$  doped with  $\text{Mn}^{2+}$  were obtained by the slow diffusion method<sup>54</sup>. In addition to excluding  $\text{CO}_2$  to ensure proper crystal growth, as much of the free oxygen as possible was removed to prevent the oxidation of  $\text{Mn}^{2+}$  to  $\text{Mn}^{3+}$  in solution. The steps involved in the preparation were as follows.

- 1) To remove  $\text{O}_2$  and  $\text{CO}_2$  gases, distilled water was boiled in air and then cooled in flowing  $\text{N}_2$  atmosphere inside a polyethylene 'glove-box'.

- 2) The reagents,  $\text{CaCl}_2 \cdot 6\text{H}_2\text{O}$  and  $\text{NaOH}$ , were dried in desiccators for 6-7 days.

- 3) The reagents, in weight ratios equal to the ratio of their molecular weights, with a pinch of dopant,  $\text{MnCl}_2 \cdot 4\text{H}_2\text{O}$ , were introduced into the diffusion box inside the 'glove-box'.

- 4) To react with any free oxygen remaining, a small amount of hydroxylamine hydrochloride was introduced into each compartment of the diffusion box. The lid was then sealed keeping  $\text{N}_2$  atmosphere above the solution.

5) As a further precaution, the diffusion box was removed from the 'glove-box' and was placed in a sealed polyethylene bag which could be purged with  $N_2$  at intervals.

A typical diffusion box is shown in Fig. IV. 2. The procedure above had to be repeated several times before crystals of a suitable size and dopant concentration were obtained. Well-formed, transparent, hexagonal, crystals of dimensions 4mm x 4mm x 3mm developed in about 8 weeks. Steps (1), (3), and (4) were repeated for separate solutions containing  $CoCl_2$ ,  $CuCl_2$ ,  $NiCl_2$ ,  $GdO_3$ , and  $EuO_2$  (some of these were first dissolved in HCl) as dopants. The characteristic EPR spectra of each ion has since been seen in their respective crystals at  $LN_2$  temperature.

Unfortunately, it proved impossible to obtain suitable  $Ca(OD)_2:Mn^{2+}$  crystals. Step (1) above using heavy water proved impractical. Several attempts at introducing  $Mn^{2+}$  to the solution using  $MnCl_2 \cdot 4H_2O$  resulted in heavy oxidation of the ion to  $Mn^{3+}$ .

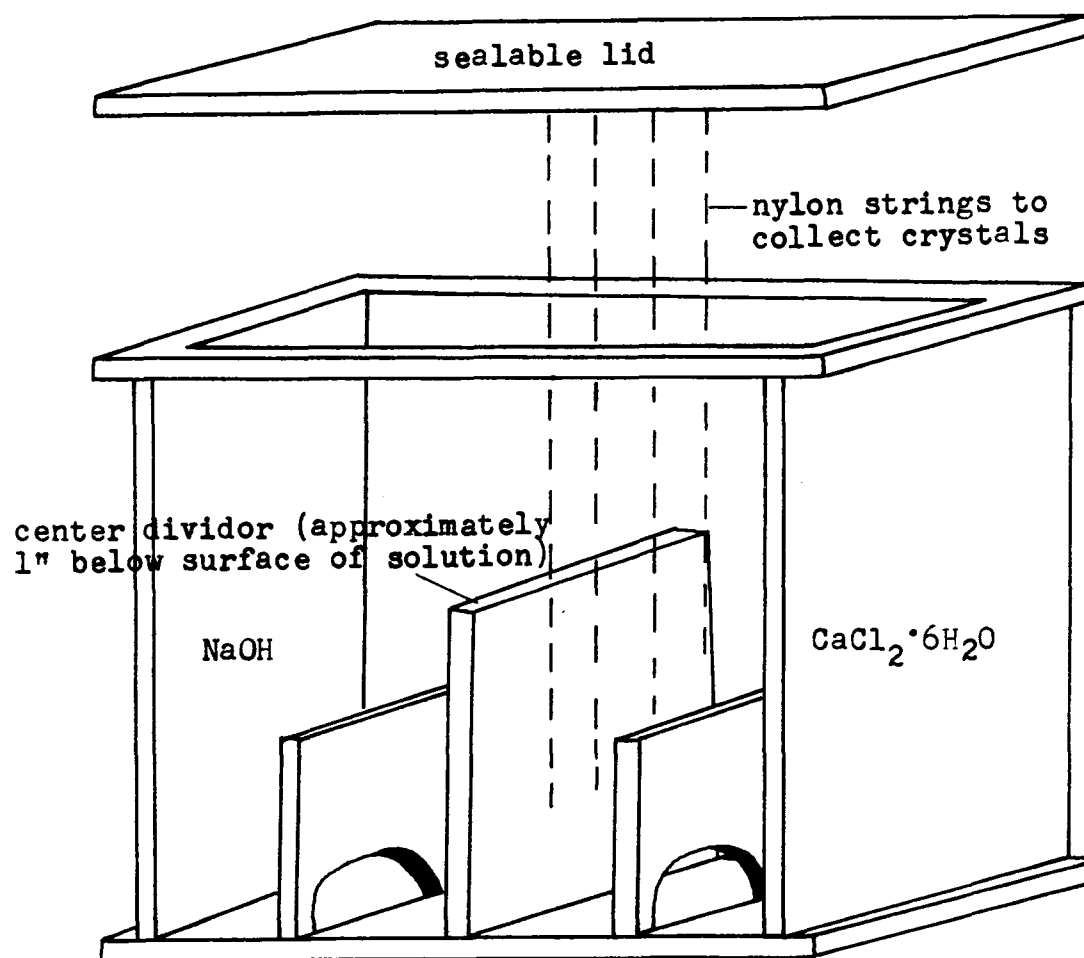


Fig.IV.2. Diffusion box used in growing  $\text{Ca}(\text{OH})_2$  crystals.

## CHAPTER V

### EXPERIMENTAL PROCEDURE AND RESULTS

#### I. ANALYSIS OF THE RT SPECTRUM

The first step in the EPR work was to identify the type of impurity in  $\text{Ca}(\text{OH})_2$  and to confirm the predictions of the crystal structure and space group. Therefore, the angular variation of the spectrum was examined by rotating the crystal in the cavity, using the crystal rotating mechanism described in Chapter IV. A stereographic projection was employed to map the polar and azimuthal angles which located the magnetic field ( $\vec{H}$ ) relative to the crystallographic axes. Typical recordings of the spectrum for  $\vec{H}$  parallel and perpendicular to the crystallographic c axis, [0001], are shown in Fig. V.3. The spectrum consisted of six groups of five lines indicative of HFS splitting larger than fine structure (FS) splitting. The spectrum was characteristic of only one  $\text{Mn}^{2+}$  ion per unit cell. Angular variations of the spectrum are given in Fig. V.1. The spectrum was isotropic for rotation of  $\vec{H}$  in the (0001) plane, and was symmetrical about the [0001] axis for rotation of  $\vec{H}$  in the (10 $\bar{1}$ 0) plane. The spectrum exhibited no symmetry for rotation of  $\vec{H}$  in the ( $\bar{1}$ 2 $\bar{1}$ 0) plane, nor in any other arbitrary plane. This behaviour is consistent with  $\text{Mn}^{2+}$  in Ca lattice sites having  $D_{3d}$  symmetry. These observations led us to choose the c axis as the magnetic z axis.

The resonant fields measured by proton MR are given in Table V.I. These measurements were used in a computer program which yielded the Hamiltonian parameters corresponding to the minimum RMS error-of-fit

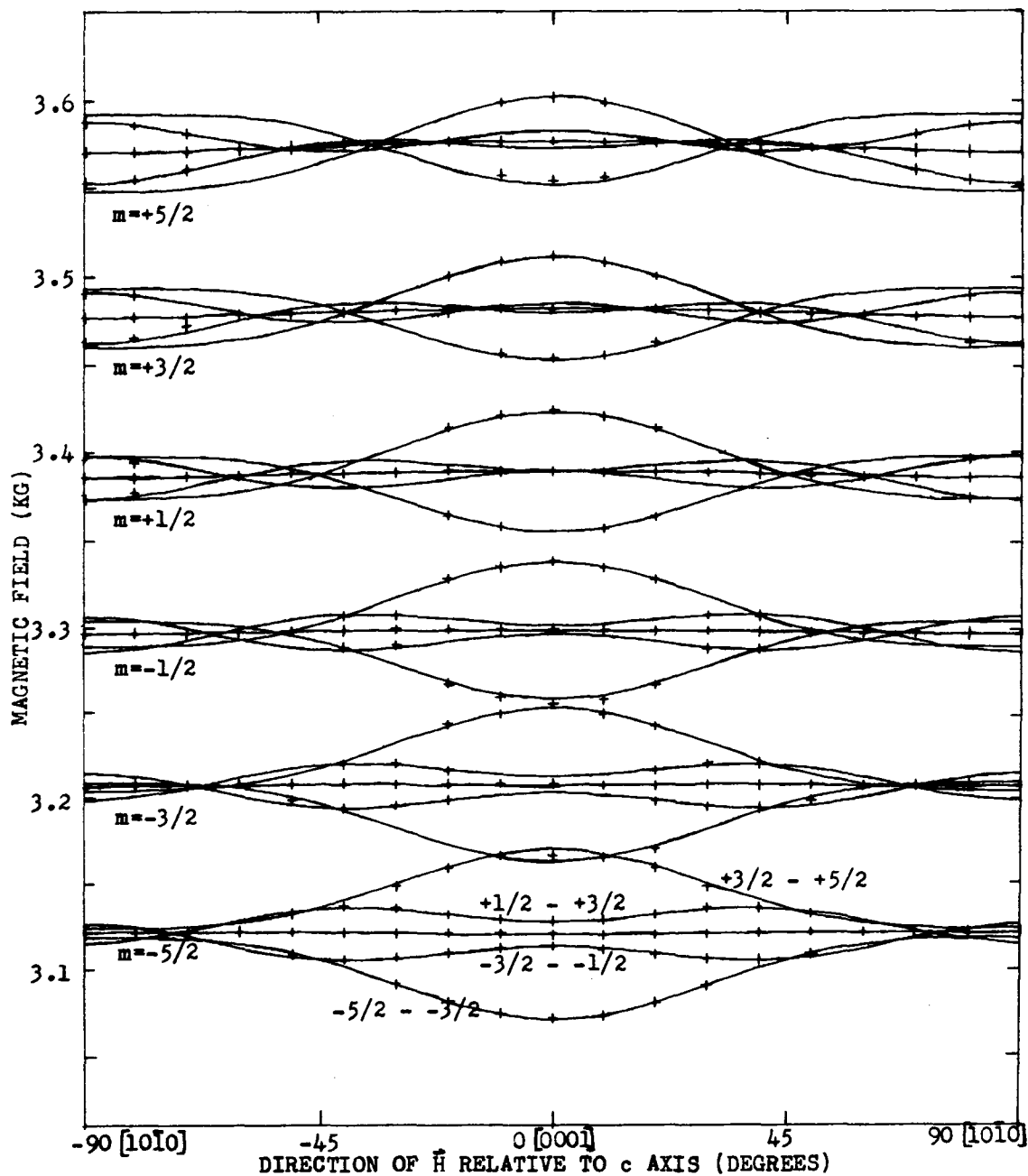


Fig.V.1a. Angular variation of spectrum for rotation of  $\vec{H}$  in  $(10\bar{1}0)$  plane.  $T=290^\circ\text{K}$ . The crosses are experimental measurements which were obtained for the microwave frequency 9380 MHz. The data for  $\vec{H} \parallel [0001]$  and  $\vec{H} \parallel [10\bar{1}0]$  are listed in Table V.1. The solid curves are plots of the formulae given in eqs.(III.3) for the values of the spin-Hamiltonian parameters given in Table V.1.

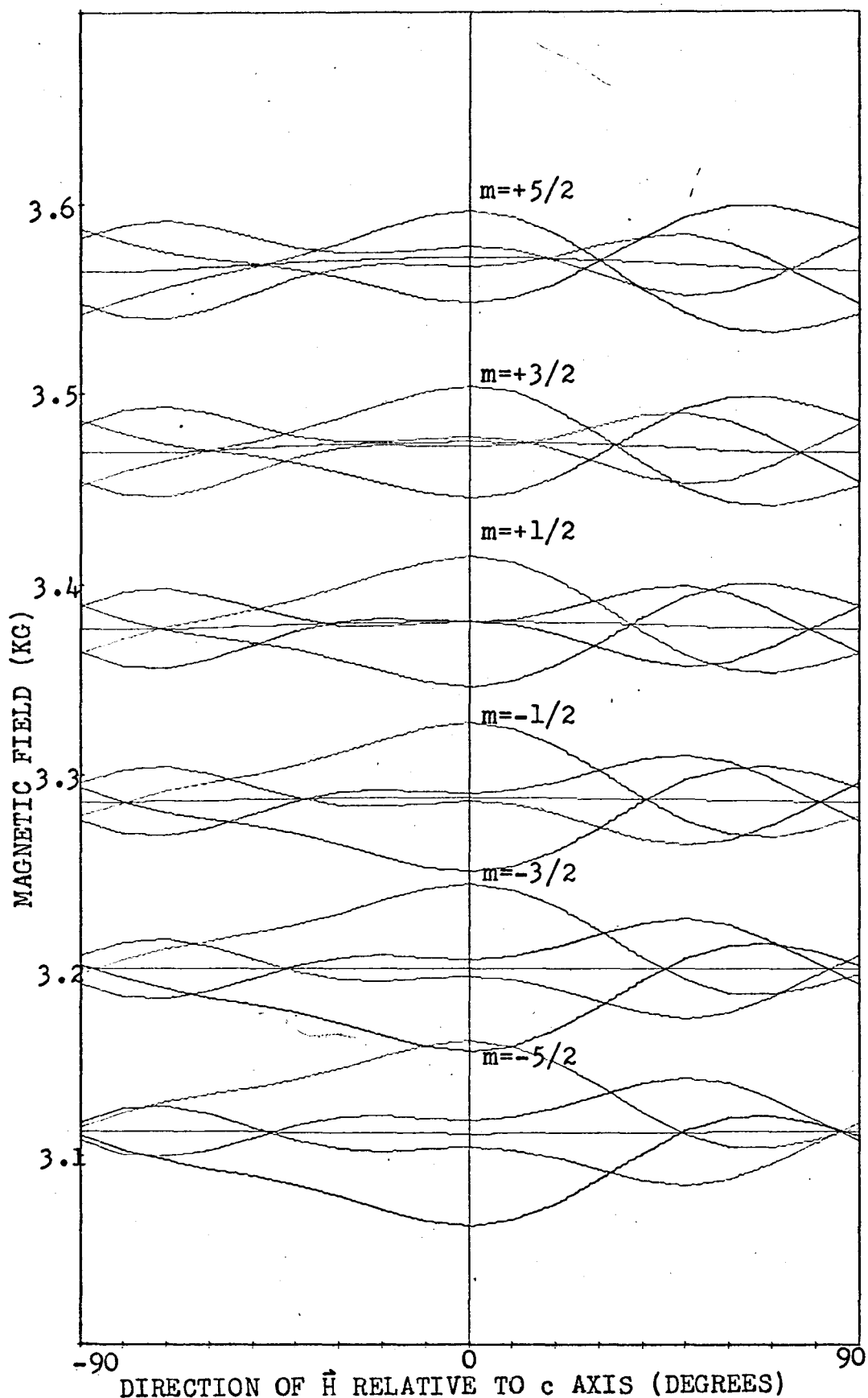


Fig.V.lb. Angular variation of spectrum for rotation of  $\hat{H}$  in  $(\bar{1}210)$  plane obtained by plotting eqs.(III.3) using the values of the spin-Hamiltonian parameters given in Table V.1 with the

TABLE V.I

Position of Resonant Fields at Room Temperature ( $290^{\circ}\text{K}$ ) and for Microwave Frequency 9380 MHz. 'Calculated' fields were computed for the Spin-Hamiltonian parameters  $g_{11} = 2.0011 \pm 0.0005$ ,  $g_{\perp} = 2.0010 \pm 0.0005$ ,  $b_2^0 = -6.7 \pm 0.5\text{G}$ ,  $b_4^0 = -2.48 \pm 0.25\text{G}$ ,  $b_4^3 = 0 \pm 100\text{G}$ ,  $A = -92.05 \pm 0.15\text{G}$ ,  $B = -90.28 \pm 0.15\text{G}$ .

Direc- tion of $\vec{H}$	TRANSITION*			MAGNETIC FIELDS IN GAUSS			
	m	M	M-1	MEASURED	CALCULATED	ERROR	
[0001]		-3/2	-5/2	3062.6	3063.1	+ 0.5	
	-5/2		-1/2	-3/2	3104.6	3104.9	+ 0.3
			1/2	-1/2	3112.4	3112.0	- 0.4
			3/2	1/2	3118.9	3119.1	- 0.2
			5/2	3/2	3199.8	3199.2	- 0.6
	-3/2		1/2	-1/2	3199.8	3199.2	- 0.6
			5/2	3/2	3245.5	3243.2	- 2.3
	-1/2		1/2	-1/2	3289.0	3288.8	- 0.2
			5/2	3/2	3328.4	3328.0	- 0.4
	1/2		1/2	-1/2	3380.8	3380.9	+ 0.1
			5/2	3/2	3415.6	3415.1	- 0.5
	3/2		-3/2	-5/2	3446.0	3445.9	- 0.1
			1/2	-1/2	3474.9	3475.3	+ 0.4
			5/2	3/2	3505.1	3504.8	- 0.3
	5/2		-3/2	-5/2	3549.1	3547.7	- 1.4
			1/2	-1/2	3571.4	3572.3	- 0.9
		5/2	3/2	3596.2	2596.8	+ 0.6	

Direc- tion of $\hat{H}$	TRANSITION*			MAGNETIC FIELDS IN GAUSS		
	m	M	M-1	MEASURED	CALCULATED	ERROR
[10 $\bar{1}$ 0]	-5/2	1/2	-1/2	3113.2	3113.3	+ 0.1
	-3/2	1/2	-1/2	3198.2	3198.6	+ 0.4
		-3/2	-5/2	3291.5	3293.7	+ 2.2
	-1/2	1/2	-1/2	3286.7	3286.4	- 0.3
		5/2	3/2	3280.5	3279.3	- 1.2
		-3/2	-5/2	3386.6	3388.9	+ 2.3
	1/2	1/2	-1/2	3376.7	3376.6	- 0.1
		3/2	1/2	3366.5	3364.1	- 2.4
		-1/2	-3/2	3483.5	3484.5	+ 1.0
	3/2	1/2	-1/2	3469.4	3469.4	0.0
		3/2	1/2	3455.7	3454.4	- 1.3
		-1/2	-3/2	3582.4	3582.3	- 0.1
	5/2	1/2	-1/2	3564.5	3564.7	+ 0.2
		3/2	1/2	3547.3	3547.1	- 0.2

\* Quantum numbers were assigned to the lines on the basis of the work of Pieczonka et al.<sup>55</sup> on Mn<sup>2+</sup> impurity in natural Brucite, Mg(OH)<sub>2</sub>, which has a structure isomorphous with Ca(OH)<sub>2</sub>.

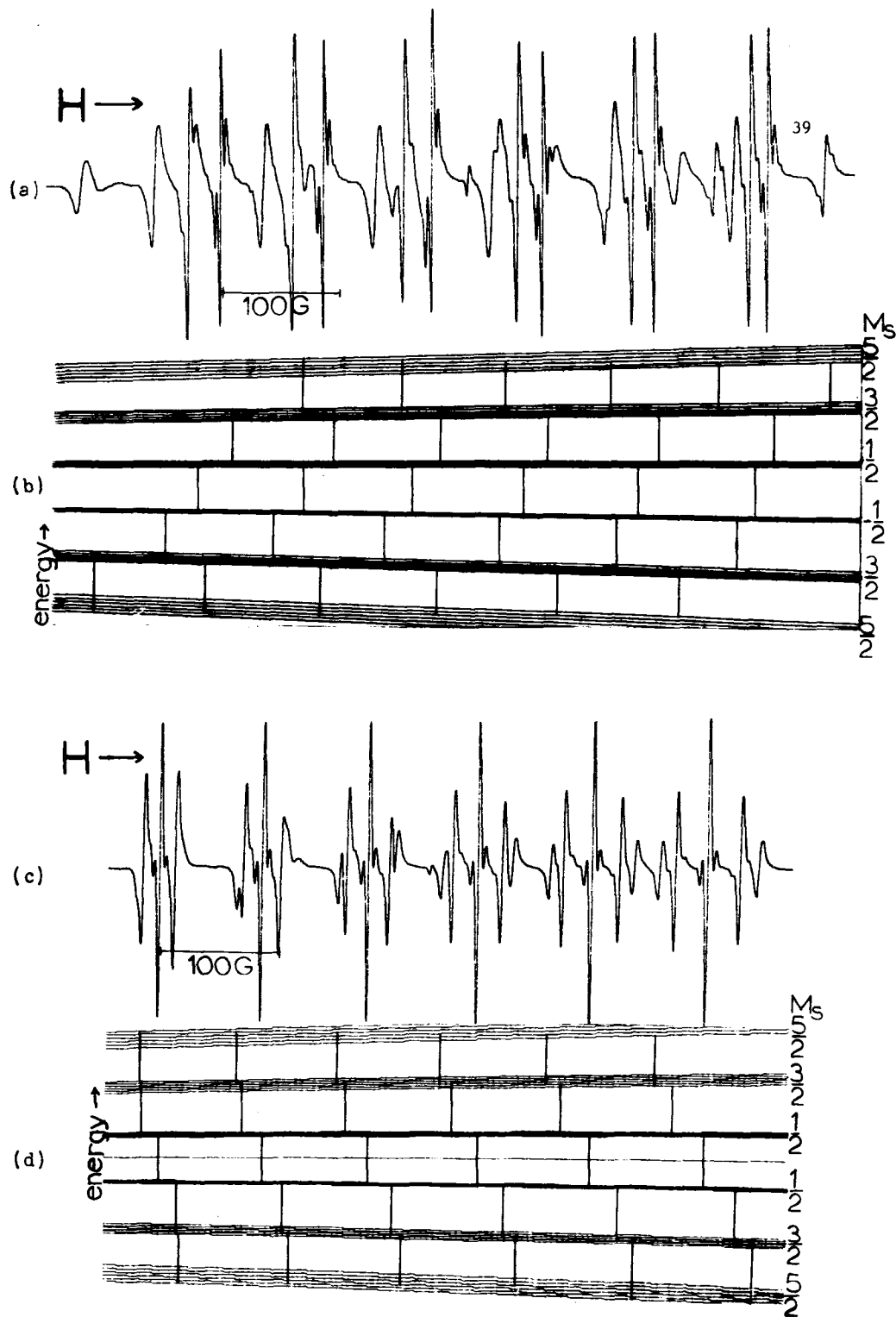


Fig.V.2. Typical recordings of the spectrum at  $T=96^{\circ}\text{K}$ . (a) Recording for  $\vec{H} \parallel [0001]$ . (b) Energy level diagram for  $\vec{H} \parallel [0001]$ . (c) Recording for  $\vec{H} \parallel [1010]$ . (d) Energy level diagram for  $\vec{H} \parallel [1010]$ . Hyperfine  $m$  quantum numbers for each type of  $\Delta M_s = \pm 1$  transition read  $-5/2$  to  $+5/2$  from left to right. Eigenvalues were plotted by computer from eqs.(III.2).

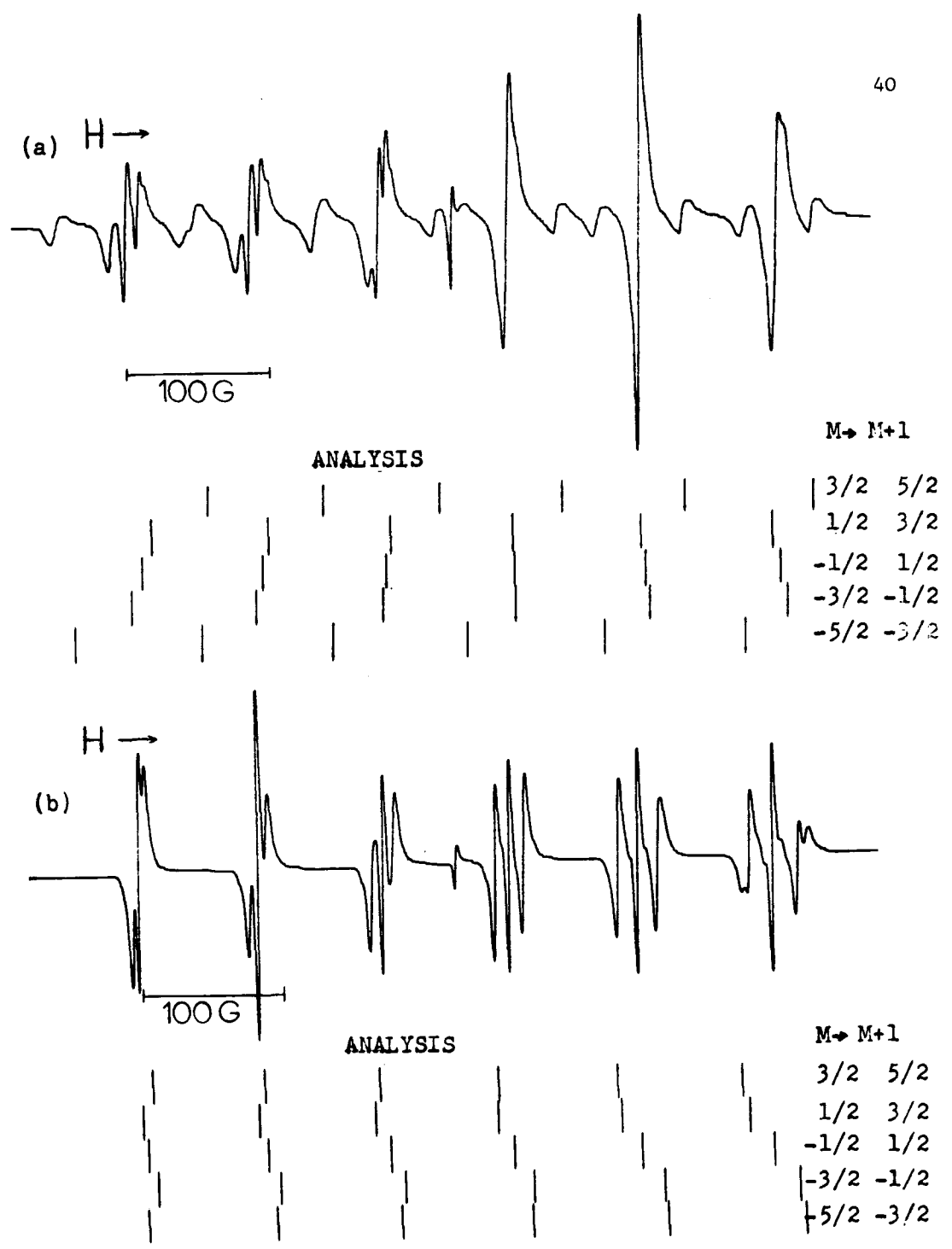


Fig.V.3. Typical recordings of the spectrum at RT. (a)  $H \parallel [001]$ .  
 (b)  $H \parallel [1010]$ .

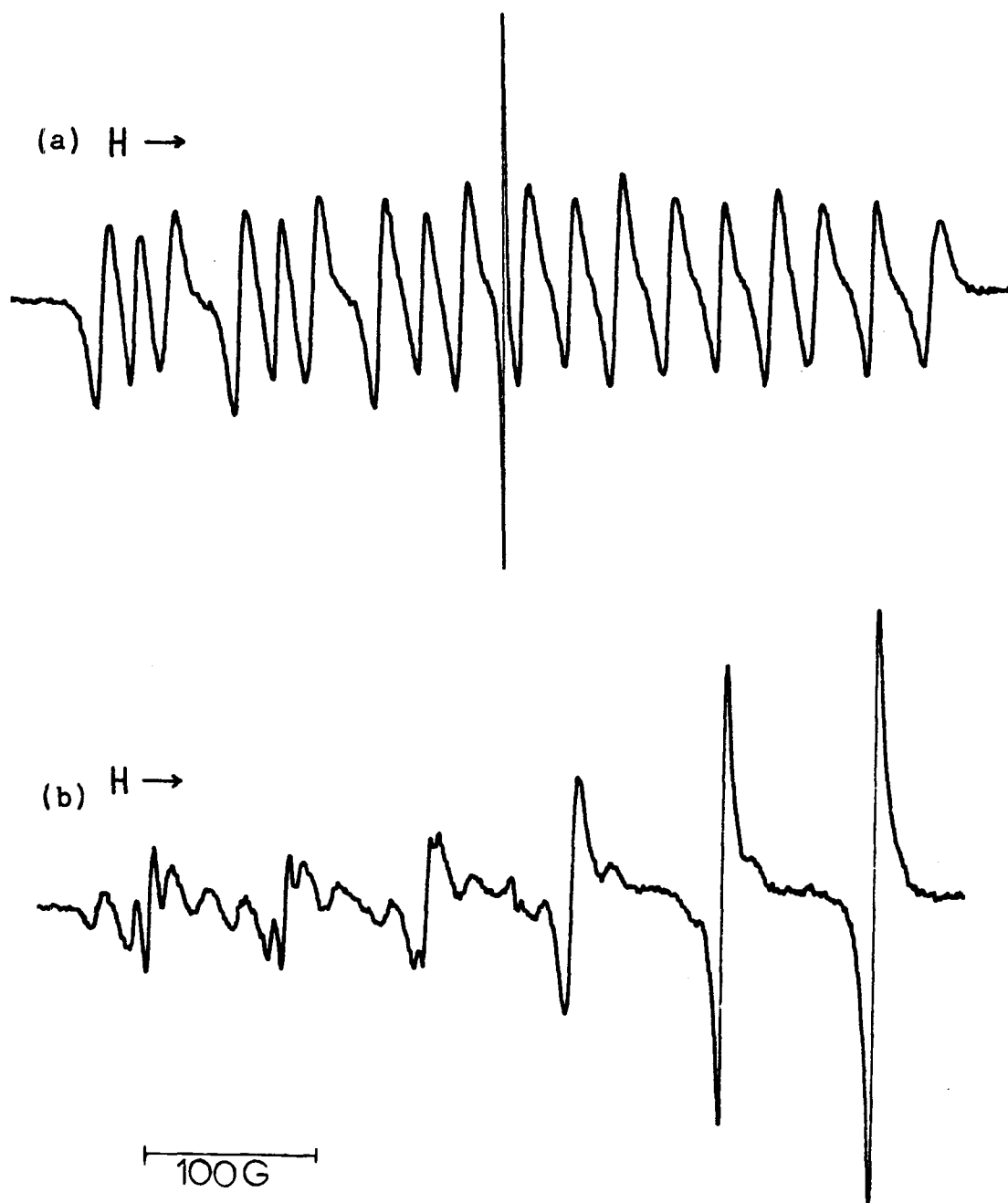


Fig.V.4. Typical recordings of the spectrum at  $609^{\circ}\text{K}$ . (a)  $\text{H} \parallel [000\bar{1}]$ . (b)  $\text{H} \parallel [10\bar{1}0]$ . The sharp central line in (a) is the resonance of the free radical dpph.

between the measured resonant fields and the calculated resonant fields.

These parameters, are also included in Table V.I. They give an RMS error of 0.78G for 27 lines.

## II. THE FS AND HFS SPECTRUM AS A FUNCTION OF TEMPERATURE

In Figs. V.2 and V.4 we present recordings of the spectrum at temperatures  $96^{\circ}\text{K}$ . and  $609^{\circ}\text{K}$ ., respectively. The spectra shown here and the ones shown in Fig. V.3 indicate that, as the temperature of the crystal varies from  $\text{LN}_2$  temperature, through RT, to  $609^{\circ}\text{K}$ ., the FS components of each HFS line reverse their order. For example, the FS components of the  $m = -5/2$  line, for  $\text{H}\downarrow\text{c}$ , crossed over each another at about RT, whereas those of the  $m = +5/2$  line did not do so until about  $609^{\circ}\text{K}$ .. The FS components of the other HFS lines crossed over one another at temperatures between these two. This behaviour indicates that  $b_2^0$  reverses sign.

The stability of the bridge spectrometer and cavity system was such that over the temperature range  $\text{LN}_2$ - $800^{\circ}\text{K}$ . the spectrum could be observed at all times on the oscilloscope. At no time did the spectrum undergo abrupt changes which would be indicative of discontinuous changes in a Hamiltonian parameter. The spectrum was visible and still reversible for temperatures of short duration up to about  $825^{\circ}\text{K}$ .. (see Fig. V.5). At temperatures in this region and above, however, the spectrum gradually died out and did not return upon cooling. When the crystal cooled from these high temperatures, it was observed to be partially decomposed into a white powder, presumably  $\text{CaO}$ . No EPR lines characteristic of the  $\text{CaO}:\text{Mn}^{2+}$  system were observed in this white powder above RT.

In 5 experimental runs, the spectrometer-cavity system was stabilized at 30 different temperatures. At each temperature the resonant fields were measured by proton MR. The results were used to compute the



Fig.V.5. Recording of the spectrum at  $T=825^{\circ}\text{K}$ .

Hamiltonian parameters by the method described in the previous section. The results for  $b_2^0$ ,  $b_4^0$ , A and B are given in Figs. V.6, V.7, and V.8, respectively. The fit was so insensitive to variations of  $b_4^3$  that no meaningful temperature dependence of this parameter was obtained. The g-value remained constant to within the experimental error,  $\pm 0.0005$ , over the whole temperature range.

#### A. Temperature Dependence of the Crystal Field Parameters

Fig. V.6 shows that at temperatures higher than about  $150^\circ\text{K}$ ., the experimental curve is essentially linear. At low temperatures the curve tapers off to approach, with zero slope, the value  $-16.25\text{G}$  at  $T=0^\circ\text{K}$ . This value has been extrapolated assuming the crystal does not undergo a phase change below  $\text{LN}_2$  temperature.

The curve labelled 'a' is a plot of the D function predicted by SDO, given by Eq. (III.5), corrected to units of gauss. Two important assumptions were made, (1) that the anion-cation distance is  $R_0$  (the Ca-O distance), and (2) that the oxygen possesses one electronic charge. Temperature dependences of  $R_0$  and  $\gamma$  were computed from the data in Table II.I.

The fitting of Eq. (III.17) to the experimental curve was simplified by first computing approximate values of  $D_0, K_1$  and  $K_2$ . A straight line visual fit to the high temperature data was drawn, the line labelled 'b' in Fig. V.6, and from it the intercept,  $-21.50\text{G}$ , and slope,  $4.95 \times 10^{-2} \text{G/K}$ , was obtained. Since the high temperature approximation of Eq. (III.17) is

$$D(T) = D_0 + \left( \frac{4.97 \times 10^{-42} K_1}{196} + \frac{11.3 \times 10^{-42} K_2}{172} \right) T,$$

we have the relations

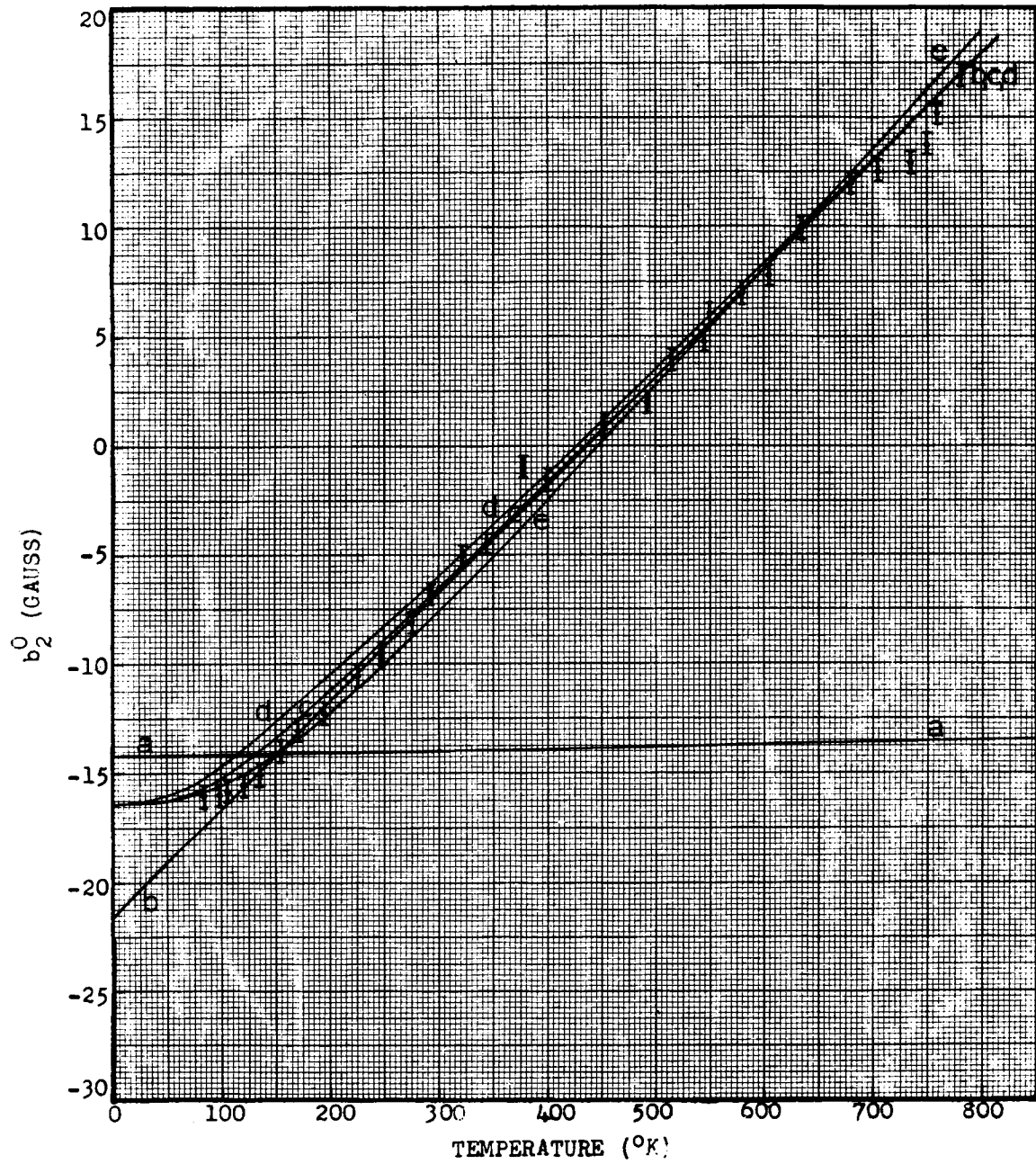


Fig.V.6.  $b_2^0$  vs. temperature. Curves labelled 'a', 'b', 'c', 'd', and 'e' are explained in the text.

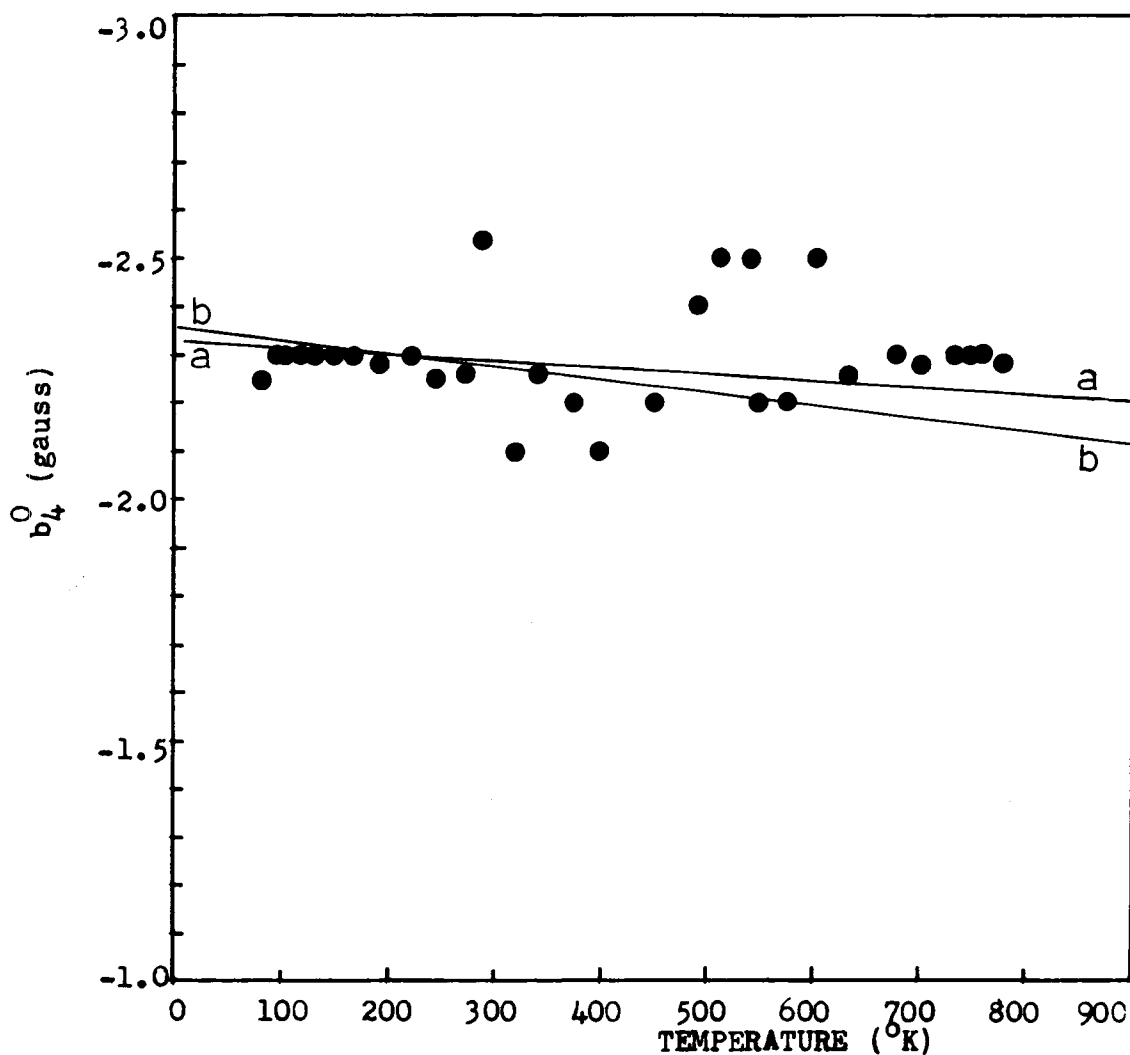


Fig.V.7.  $b_4^0$  vs. temperature. Possible errors in the data are  $\pm 0.25G$ . Curves 'a' and 'b' are plots of the functions  $b_4^0 = M_1 R_0^{-5}$  and  $b_4^0 = M_2 R_0^{-10}$  where  $M_1 = -4.12 \times 10^3$  and  $M_2 = -7.40 \times 10^6$ . Units of  $M_1$  and  $M_2$  are gauss  $\times a_0^5$  and gauss  $\times a_0^{10}$  where  $a_0$  is the Bohr radius. These functions represent typical mechanisms which have been proposed for the parameter  $a$  taken from Table III.1.

$$D_0 = -21.50G ,$$

$$\text{and } \frac{4.97}{196} \times 10^{-42} K_1 + \frac{11.3}{172} \times 10^{-42} K_2 = 4.95 \times 10^{-2}$$

In addition, the  $T=0$  approximation of Eq. (III.17) gives

$$D_0 + 4.97 \times 10^{-42} K_1 + 11.3 \times 10^{-42} K_2 = -16.25$$

so that by solving these equations we obtained the values

$$D_0 = -21.50 \pm 0.50G, K_1 = (5.38 \pm 0.5) \times 10^{42} \text{G/erg-sec}^2 \text{ and } K_2 = (2.83 \pm 0.5) \times 10^{42} \text{G/erg-sec}^2.$$

A plot of Eq.(III.17) using these values is shown as curve 'c' in Fig.V.6.

An attempt was made to improve on these values by using them as zeroth order approximations in a best fit program. The results however, gave a curve which favoured the low temperature data while giving a poor fit to the high temperature data. The quantities  $D_0$ ,  $K_1$  and  $K_2$  quoted above give the best fit of Eq. (III.17) over the whole temperature range.

Since the temperature dependences of  $b_2^0$  and of  $A$  were qualitatively similar, an expression for  $b_2^0$ , of the same form as that for  $A$ , given by Eq. (III.18), was also fitted to the experimental data. Normalizing the two curves at  $636^\circ\text{K}$ . and using the values  $b_2^0(0) = -16.25G$ ,  $\theta = 260^\circ\text{K}$ . we obtained the value  $5.07 \times 10^{-10} \text{K}^{-4}$  for the constant  $C$  in Eq.(III.18). These values give curve 'd' in Fig. V.6. A slightly better fit at low and high temperatures was obtained for the values  $b_2^0(0) = -16.25G$ ,  $\theta = 500^\circ\text{K}$ ., and  $C = 8.28 \times 10^{-11} \text{K}^{-4}$ . This is curve 'e' in Fig. V.6.

The method of using a best fit program to derive the Hamiltonian parameters resulted in a non-uniform variation of  $b_4^0$  values as seen in Fig. V.7. The RMS error of fit was far more sensitive to variations in

$b_2^0$ , A and B than in  $b_4^0$ . Thus it was impossible to define an accurate fit to the data. The curves labelled 'a' and 'b' represent the functions  $b_4^0 = M_1 R_0^{-5}$  and  $b_4^0 = M_2 R_0^{-10}$ , respectively, where  $M_1$  and  $M_2$  are constants. These functions were normalized to the value of  $b_4^0 = -2.3G$  at  $T = 200^\circ K$ .

#### B. Temperature Dependence of the Hyperfine Parameters

The temperature dependences of A and B have been given in Fig.V.8. We have not attempted a theoretical analysis of A(T) and B(T) taken separately. Qualitatively, the curves were similar. The quantity  $\eta = \left| \frac{(A^2 - B^2)^{1/2}}{A} \right|$ , taken from the data of Fig. V.8, is shown as a function of temperature in Fig. V.9. A straight line visual fit to the data is indicated. The rate at which  $\eta$  decreased, given by the slope of this line, was of the order of  $7.6 \times 10^{-5} \text{ }^\circ K^{-1}$ . The temperature dependence of the quantity  $(A+2B)/3$ , obtained from the data of Fig. V.8, is given in Fig. V.10. Eq.(III.18) was fitted to the experimental curve by evaluating the integral numerically and normalizing the theoretical curve and experimental curve at  $600^\circ K$ . The best fit for a Debye Temperature of  $260^\circ K$  was obtained for  $A(0) = -92.05G$  and  $C = 10.6 \times 10^{-12} \text{ }^\circ K^{-4}$ . A plot of Eq. (III.18) for these constants is the curve labelled 'a' in Fig. V.10. The best overall fit to the data, however, was obtained for  $A(0) = -92.00G$ ,  $\theta = 500^\circ K$ , and  $C = 1.78 \times 10^{-12} \text{ }^\circ K^{-4}$ . These values give the curve labelled 'b' in Fig. V.10.

### III. $Mn^{2+}$ -H SHFS AND GENERAL DISCUSSION OF LINESHAPES

The  $Mn^{2+}$ -H SHFS was studied in the  $(10\bar{1}0)$  plane at a temperature of  $85^\circ K$  and for H $\parallel$ c in the range  $80-130^\circ K$ .

Fig. V.11 shows SHFS splittings of the FS components of the

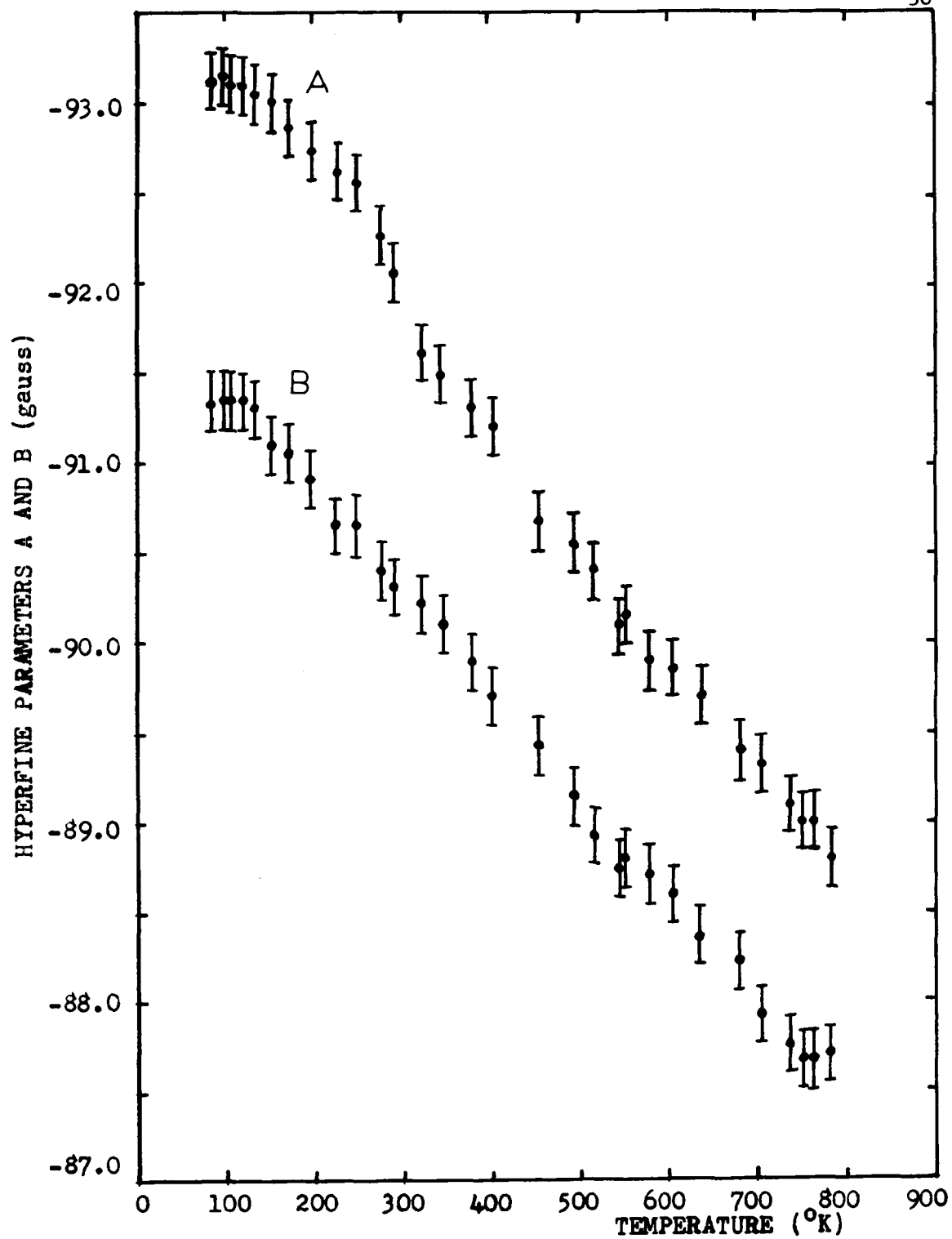


Fig.V.8. A and B vs. temperature.

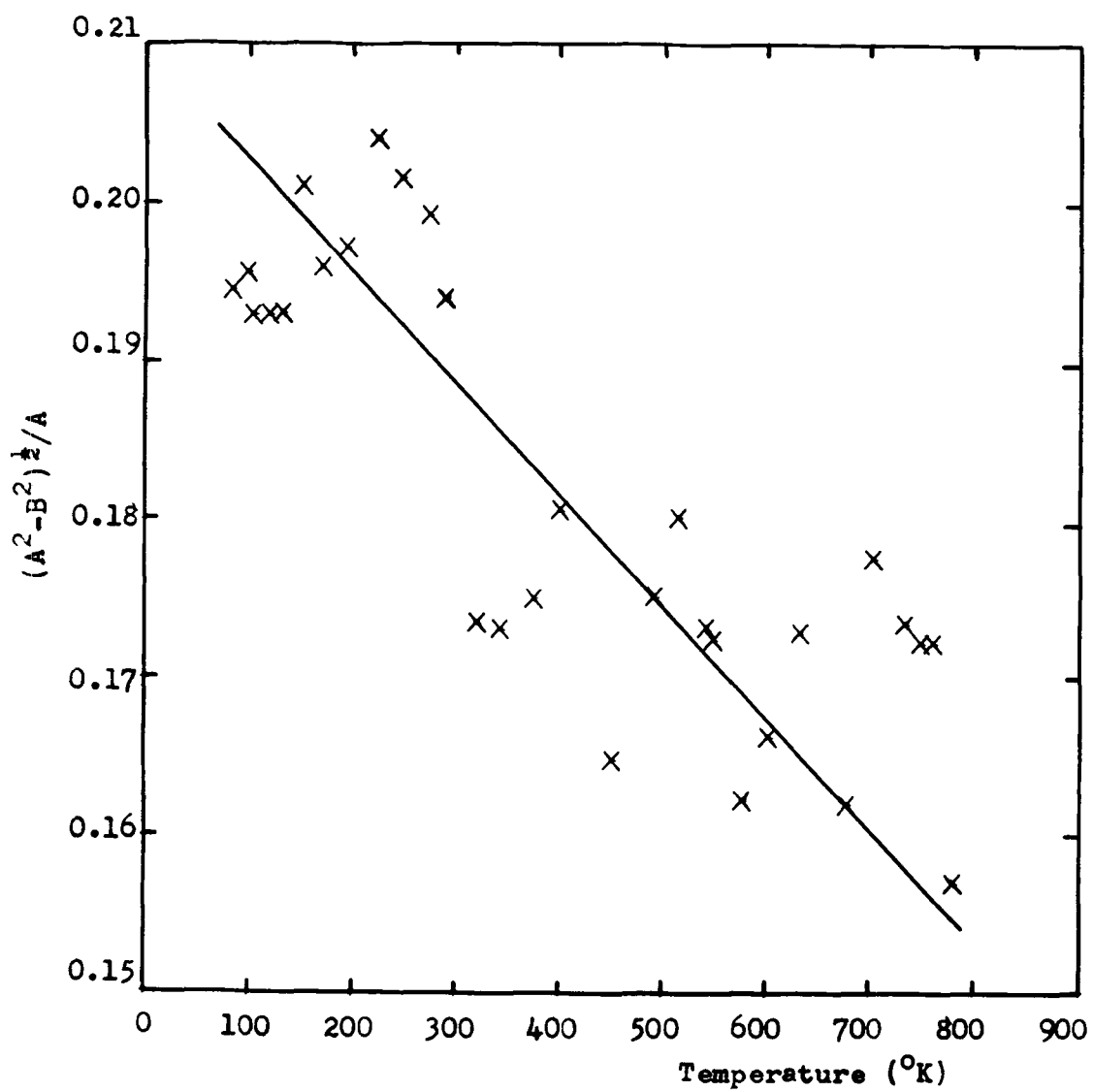


Fig.V.9.  $\eta = \left| \frac{(A^2 - B^2)^{\frac{1}{2}}}{A} \right|$  vs. temperature. The data are listed in Appendix B.

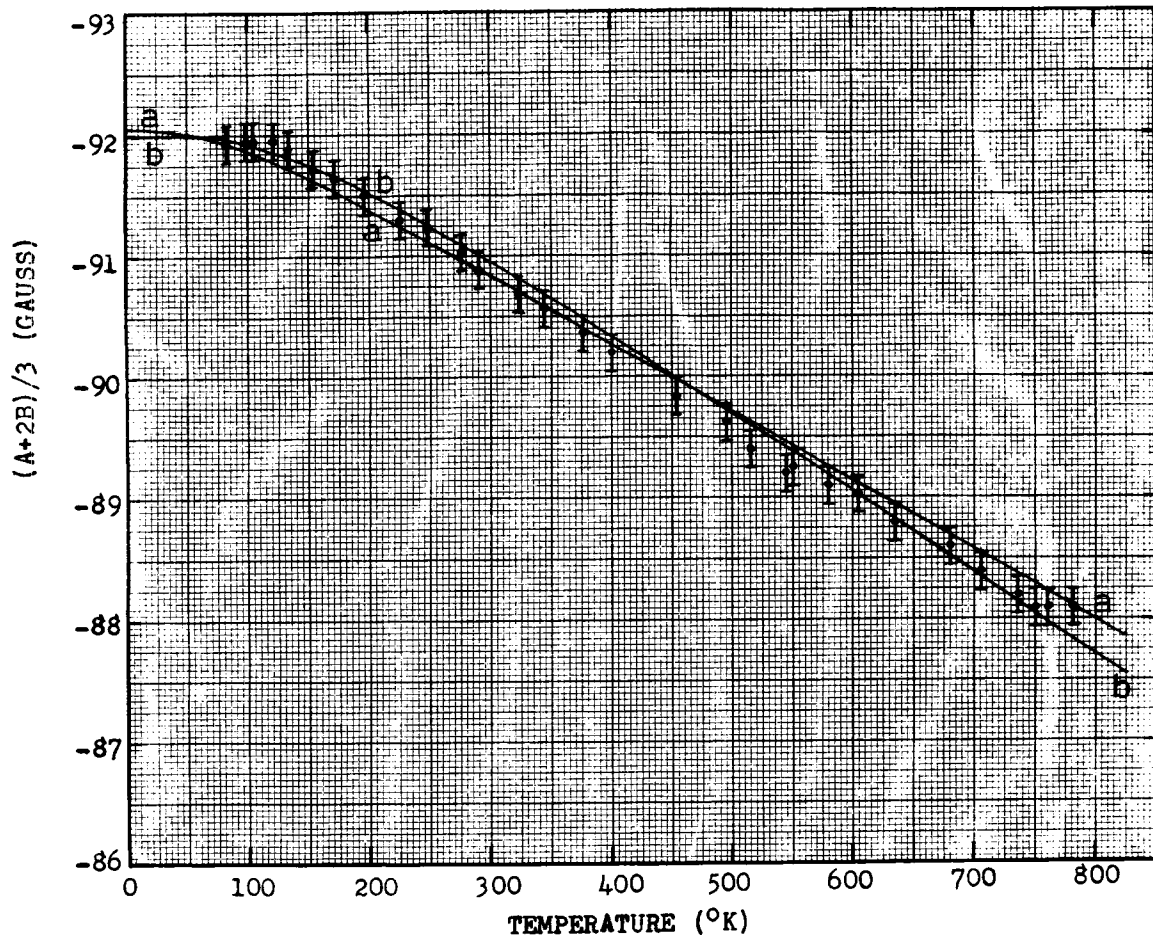


Fig.V.10.  $(A+2B)/3$  vs. temperature. Data are listed in Appendix B.

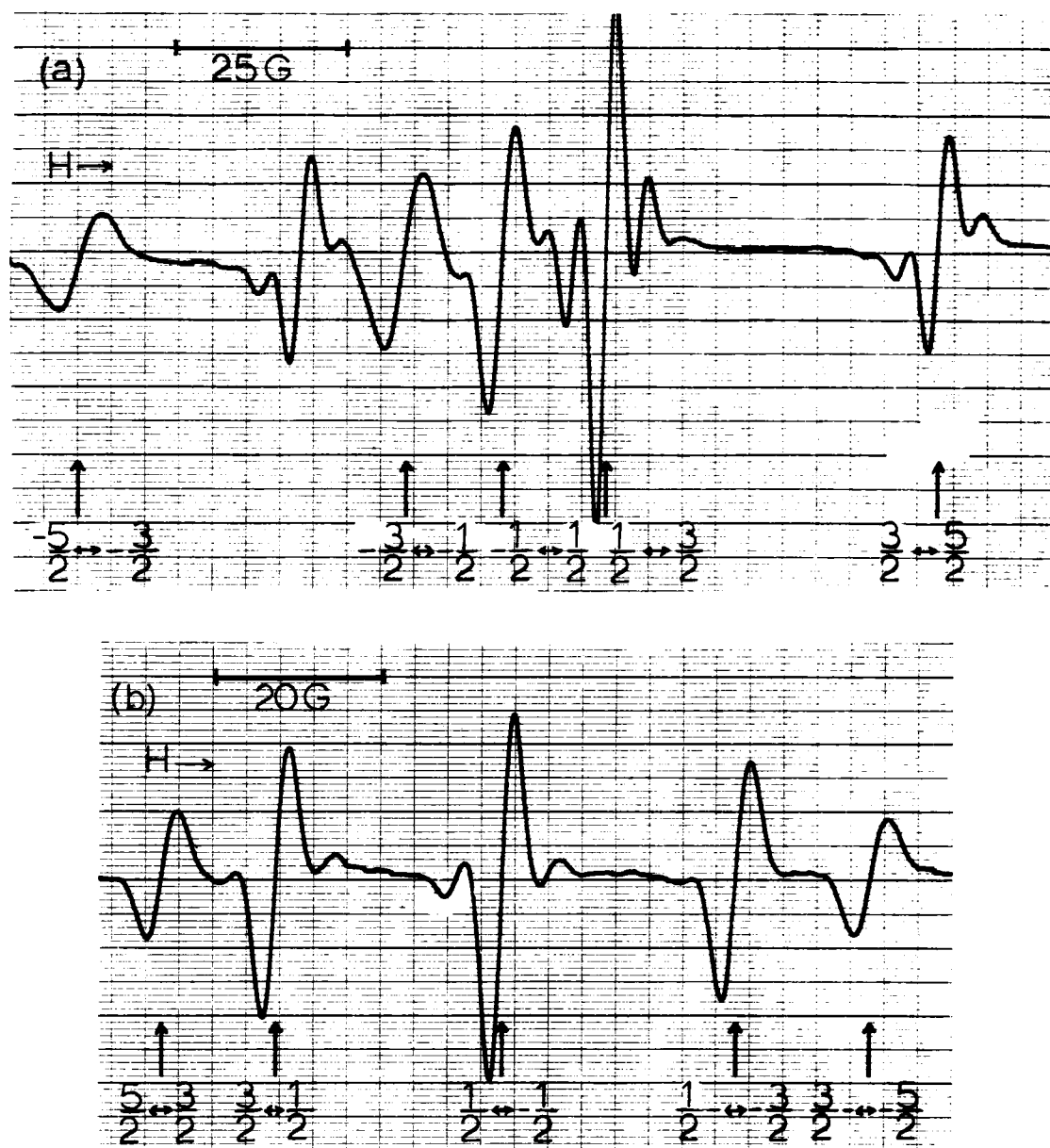


Fig.V.11. FS components of the  $m=+5/2$  hyperfine line.  
 (a)  $\vec{H} \parallel [0001]$  . (a)  $\vec{H} \parallel [1010]$  .

$m = +5/2$  hyperfine line. The physical properties of the corresponding FS components of the other hyperfine lines were similar, as can be seen from Fig. V.2. For both orientations of  $\hat{H}$ , the FS components were displaced symmetrically about the  $M_s: -\frac{1}{2} \leftrightarrow +\frac{1}{2}$  line. For  $\hat{H} \parallel c$  the intensity ratios were approximately 5:11:15:11:5 (taking peak-to-peak heights as proportional to the line intensities, which is true if the line widths are the same). For  $\hat{H} \parallel c$  the intensity ratios were approximately 5:8.7:14:27:11 but the line widths were not equal. Neglecting SHFS the ratios should be 5:8:9:8:5. The broadest line at  $85^\circ\text{K}$  was of the order 6G wide. This was the  $M_s: -5/2 \leftrightarrow -3/2, m = 5/2$  line with unresolved SHFS for  $\hat{H} \parallel c$ .

Fig V.11 shows that not all FS components were split equally. For  $\hat{H} \parallel c$  correspondingly displaced FS lines were split equally. For  $\hat{H} \parallel c$ , however, the  $M_s: +3/2 \leftrightarrow 1/2$  line was split the most, followed by the lines  $M_s: 5/2 \leftrightarrow 3/2, M_s: 1/2 \leftrightarrow -1/2$ , and then the rest, which showed no resolved structure at all.

Fig. V.12 shows the  $M_s: 1/2 \leftrightarrow 3/2, m = -5/2$  line for  $\hat{H} \parallel c$  at low ( $\sim 1\text{mW}$ ) and high ( $\sim 50\text{mW}$ ) power levels. At low power a 5 line spectrum was fully visible. At high power there existed just a hint of a 7 line spectrum. The central component showed some saturation at high power (full power from an X13 Klystron) at  $85^\circ\text{K}$ . The approximate intensity ratios at low power were  $x:5:37:95:39:7:x$  ( $x$  was unknown at low power) as compared with the theoretical ratios 1:6:15:20:15:6:1. From chart recordings obtained at high power (Fig. V.12) the components were observed to be equally spaced by approximately 4G.

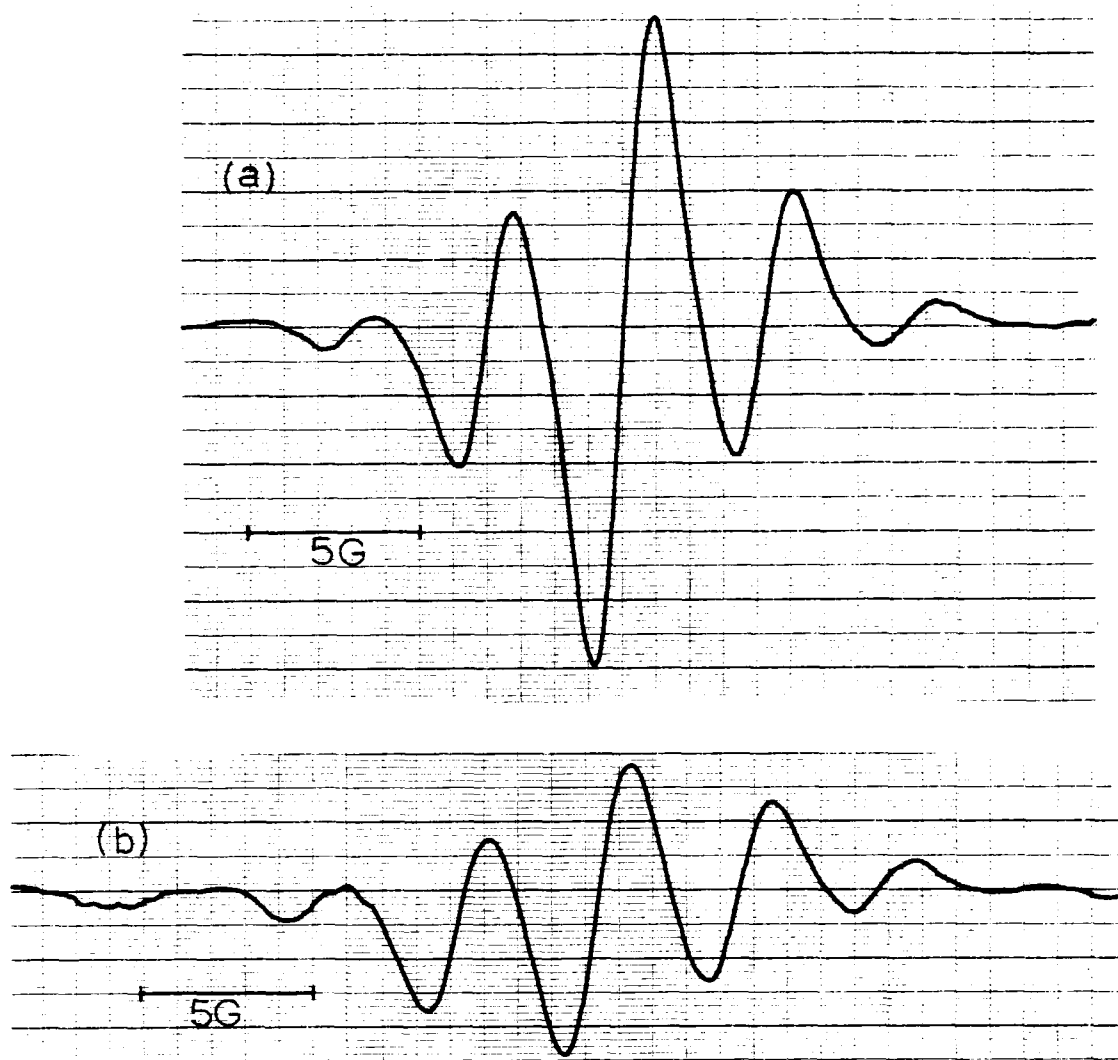


Fig.V.12. The  $M_s: 1/2 \leftrightarrow 3/2; m = -5/2$  line at low and high power levels. (a) low power ( $\sim 1$  mW). (b) high power ( $\sim 50$  mW).

The angular variation of the relative SHFS splitting between the central component and the first components on either side of the central component is shown in Fig. V.13. Each point is the mean of about 12 separate measurements, the 'upper' and 'lower' splittings of the FS components of each of the 6 hyperfine lines. Data are missing between about  $20^\circ$  and  $65^\circ$  due to slight broadening and considerable overlapping of the lines. A dependence of this splitting on  $M_s$  is evident from the figure. There also appears to be a slight anisotropy. The mean value of the splitting for  $\vec{H} \parallel c$  indicates  $A_s \sim 4.5G$ . Finally, the temperature dependence of the relative SHFS splittings was linear, within the experimental error, in the range  $80^\circ K$ - $130^\circ K$ . Above  $130^\circ K$  SHFS splittings were obscured by slight broadening and overlapping of the lines.

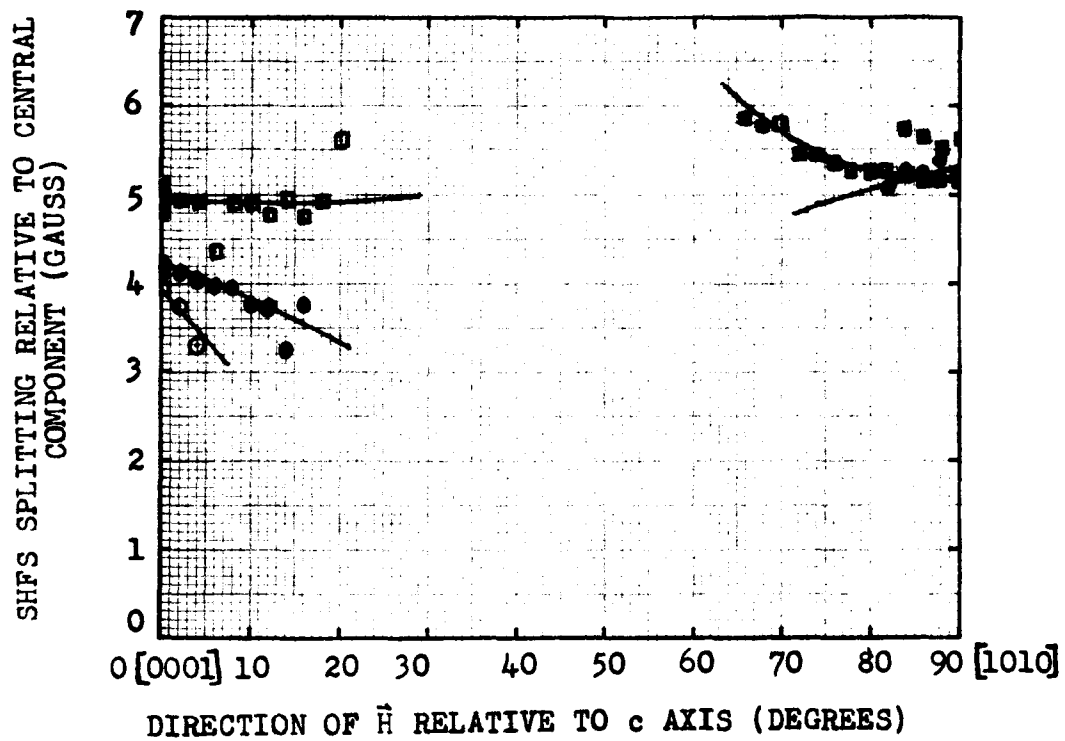


Fig.V.13. Angular variation of SHFS splitting relative to the central component. Rotation of  $H$  is in  $(10\bar{1}0)$  plane.  
 Legend:  $\circ$  -  $3/2 \leftrightarrow 5/2$  FS component;  $\bullet$  -  $1/2 \leftrightarrow 3/2$  FS component;  
 $\square$  -  $-1/2 \leftrightarrow 1/2$  FS component;  $\blacksquare$  -  $-3/2 \leftrightarrow -1/2$  FS component.

## CHAPTER VI

### DISCUSSION AND CONCLUSIONS

The temperature dependences of the spin-Hamiltonian parameters showed no discontinuities in the temperature range 85°K-800°K. We can conclude, therefore, that the  $\text{Ca}(\text{OH})_2$  crystal remained stable in the trigonal phase in this range. The fact that the crystal began to decompose at temperatures of 800°K and above, is consistent with the fact that its dissociation pressure reaches 1 atm. at 785°K.<sup>56</sup> The  $\text{Mn}^{2+}$  probably oxidized to  $\text{Mn}^{3+}$  during this dehydration reaction since no EPR lines were observed in the powder product of the dehydration.

The  $b_2^0(T)$  which was predicted from the theory of SDO (curve 'a' in Fig. V.6) coincided with the  $b_2^0$  which was measured experimentally at 150°K. Also, the value of  $b_2^0(0) = -14.25\text{G}$ , which was predicted by this theory, differed by only 2G from the value of  $b_2^0(0) = -16.25\text{G}$  which was extrapolated from the experimental data. We conclude, therefore, that the SDO theory gives a good fit to the experimental data at low temperatures. It is possible that a better fit could have been obtained had the OH group been treated as a dipole, instead of as a point charge located on the oxygen, and had a more accurate value of the anion-cation bond distance been determined. The value of  $B_2^0$  in the point-charge computation could also be improved by summing eq. (III.6) over many neighbours. In any case, the theoretical function  $b_2^0(T)$  should remain a linear function of temperature

because of the thermal expansion of R.

Proceeding on the assumption that the  $b_2^0(T)$  predicted by SDO is the correct explanation of the experimental  $b_2^0(T)$  at low temperatures, the experimental  $b_2^0(T)$  should have followed the curve 'a' in Fig. V.6 at high temperatures, if the temperature dependence were determined only by the thermal expansion of R. The fact that the two curves differed markedly at high temperatures implies that thermal expansion is not of major importance in the experimental  $b_2^0(T)$ . Unfortunately we were not able, in a simple manner, to estimate the contribution of thermal expansion to the data. This is only possible when the spin-Hamiltonian parameters are studied as a function of both temperature and pressure.<sup>37</sup> The fact that the  $b_2^0(T)$  predicted from the theory of Walsh, Jeener, and Bloembergen<sup>37</sup>, given by Eq. (III.17), gave a good fit to the data shows that discrete lattice modes can account for the experimental  $b_2^0(T)$ . The assumption that the T' modes transforming as  $A_{1g}$  and  $E_g$  in  $D_{3d}$  symmetry are the modes most responsible for the temperature dependence of  $b_2^0(T)$  thus gives satisfactory results. The fact that a curve of the form of Eq. (III.18) gave fits to the data almost as good as the above means that it is impossible to state whether the  $Mn^{2+}$  vibronic coupling is due exclusively to lattice modes of certain discrete frequencies, or to a continuous spectrum of modes describable by a Debye approximation. Both approaches appear to be equally valid.

We feel that we have been justified in applying to the data an expression for  $b_2^0(T)$  of the same form as that for  $A(T)$  which was derived by Orbach and Simanek<sup>50</sup>. The mechanisms which apply for  $b_2^0(T)$  will, of course, be different from the Fermi contact interaction which applies for

A. In any case, a function of the general form of Eq. (III.18) should result from computations involving  $W_{OL}$  since the form of Eq. (III.18) is the result of averaging the mean square strains.

Although the accuracy in the determination of  $b_4^0$  was poor, the temperature dependence of  $b_4^0$  tended to show a linear behaviour. Therefore, the effects of lattice vibrations on the experimental  $b_4^0(T)$  were probably negligible. Walsh et. al.<sup>37</sup> reached the same conclusion for the parameter  $a$ . Although the experimental  $b_4^0(T)$  tended to show a dependence, such as  $b_4^0 = CR_0^{-n}$ , where  $C$  is a constant,  $R_0$  is the Ca-O bond distance and  $n$  is some number (see Table III.1), it proved impossible to determine the value of  $n$  unequivocally.

The theory of Simanek and Orbach<sup>50</sup> gave a good fit to the isotropic part of the axially-symmetric HFS tensor. As expected, the temperature dependence of this quantity was similar to the temperature dependence of the isotropic HFS tensor of  $Mn^{2+}$  in cubic crystals<sup>50</sup>. The best fit to the data was obtained for an average Debye Temperature of  $500^\circ K$  instead of for the value of  $260^\circ K$  which was calculated from the low temperature specific heat data. We should expect an average Debye Temperature to be somewhat higher than a Debye Temperature which is derived from low temperature specific heat data since the Debye Temperature is somewhat temperature dependent. The constants of Eq. (III.18) which were determined in this work, namely,  $\theta = 500^\circ K$ ,  $C = 1.78 \times 10^{-12} K^{-4}$ , compare favourably with the values found for  $Mn^{2+}$  in CaO, namely,  $\theta = 450^\circ K$ , and  $C = 2.30 \times 10^{-12} K^{-4}$ .<sup>57</sup> The fact that  $\eta$  tended to decrease with temperature implies that the axial distortion of the HFS tensor tended to decrease with temperature. There is no

explanation in the literature to account for this effect.

The SHFS tensor was largely isotropic. The isotropic Fermi contact part was of the order of 4.5G at 85°K. The anisotropic dipolar part was probably of the order of 0.1G or less. There appeared to be a slight dependence of this splitting on  $M_s$ . This could have been the result of a second-order effect.

## REFERENCES

1. Early references are quoted by R.W.G. Wyckoff, The Structure of Crystals (Reinhold Pub. Comp., N.Y. 1931).
2. H.D. Megaw, Proc. Roy. Soc. (London), A142, 198 (1933).
3. J.D. Bernal and H.D. Megaw, Proc. Roy. Soc. (London), A151, 384 (1935).
4. Bunn, Clark, and Clifford, Proc. Roy. Soc. (London), A151, 141 (1935).
5. H.E. Petch and H.D. Megaw, J. Opt. Soc. Am., 44, 744 (1954).
6. H.E. Petch, Phys. Rev., 99, 1635 (1955).
7. H.E. Petch, Can. J. Phys., 35, 983 (1957).
8. H.E. Petch, Acta, Cryst., 14, 950 (1961).
9. H.E. Swanson and E. Tatge, Nat. Bur. Stand. Cir. 539, 1, 58 (1953).
10. W.R. Busing and H.A. Levy, J. Chem. Phys., 26, 563 (1957).
11. D.M. Henderson and H.S. Gutowsky, Am. Mineral., 47, 1231 (1962).
12. W.E. Hatton, D.L. Hildenbrand, G.C. Sinke, and D.R. Stull, J. Am. Chem. Soc., 81, 5028 (1959).
13. R.A. Buchanan, H.H. Caspers, and J. Murphy, Applied Optics, 2, 1147 (1963).
14. G. Safford, V. Brajovic, and H. Boutin, J. Phys. Chem. Solids, 24, 771 (1963).
15. I. Pelah, K. Krebs, and Y. Imry, J. Chem. Phys., 43, 1864 (1965).
16. S.S. Mitra, J. Chem. Phys. 39, 3031 (1963).
17. O. Oehler, and H.H. Gunthard, J. Chem. Phys., 48, 2036 (1968).
18. S.S. Mitra, Solid State Physics, 13, 1 (1962).
19. G.F. Koster, Solid State Physics, 5, 1 (1957).
20. O. Oehler and H.H. Gunthard, J. Chem. Phys., 48, 2032 (1968).

21. W. Low, *Phys. Rev.*, 105, 793 (1957).
22. H.A. Bethe, *Ann. Physik*, 3, 133 (1929); English translation, Consultants Bureau, New York, 1958.
23. V.M. Vinokurov, M.M. Zaripov, and V.G. Stepanov, *Soviet Phys. - Solid State*, 6, 866 (1964).
24. R. Orbach, *Proc. Roy. Soc. (London)*, A264, 458 (1961).
25. J.R. Thyer, S.M. Quick, and F. Holuj, *Can. J. Phys.* 45, 3597 (1967).
26. H.A. Buckmaster, *Can. J. Phys.*, 40, 1670 (1962).
27. M.T. Hutchings, *Solid State Physics*, 16, 227 (1964).
28. B. Bleaney and R.S. Trenam, *Proc. Roy. Soc. (London)*, A223, 1 (1954).
29. H. Watanabe, Operator Methods in Ligand Field Theory (Prentice-Hall, Inc., N.J. 1966).
30. G. Racah, *Phys. Rev.*, 63, 367 (1943).
31. R. Trees, *Phys. Rev.*, 82, 683 (1951).
32. M.H.L. Pryce, *Phys. Rev.*, 80, 1107 (1950).
33. R.R. Sharma, T.P. Das, and R. Orbach, *Phys. Rev.*, 149, 257 (1966).
34. R.R. Sharma, T.P. Das, and R. Orbach, *Phys. Rev.*, 171, 378 (1968).
35. A. van Heuvelen, *J. Chem. Phys.*, 46, 4903 (1967).
36. W.M. Walsh Jr., *Phys. Rev.*, 122, 762 (1961).
37. W.M. Walsh Jr., J. Jeener, and N. Bloembergen, *Phys. Rev.*, 139, A1338 (1965).
38. R.R. Sharma, T.P. Das, and R. Orbach, *Phys. Rev.*, 155, 338 (1967).
39. H. Watanabe, *Prog. Theoret. Phys.*, 18, 405 (1957).
40. M.J.D. Powell, J.R. Gabriel, and D.F. Johnston, *Phys. Rev. Lett.*, 5, 145 (1960).
41. J.R. Gabriel, D.F. Johnston, and M.J.D. Powell, *Proc. Roy. Soc. (London)* A264, 503 (1961).
42. W. Low and G. Rosengarten, *J. Mol. Spectr.* 12, 319 (1964).

43. W.M. Walsh Jr., Phys. Rev., 114, 1473 (1959).
44. C.C. Klick and J.H. Schulman, J. Opt. Soc. Am., 42, 910 (1952).
45. J.H. Van Vleck, J. Chem. Phys., 7, 72 (1939).
46. J.H. Van Vleck, Phys. Rev., 57, 426 (1940).
47. A. Abragam and M.H.L. Pryce, Proc. Roy. Soc., (London), A205, 135 (1951).
48. V. Heine, Phys. Rev., 107, 1002 (1957).
49. R.E. Watson and A.J. Freeman eds., Hyperfine Interactions, (Academic Press N.Y. 1967).
50. E. Simanek and R. Orbach, Phys. Rev., 145, 191 (1966).
51. M. Tinkham, Proc. Roy. Soc., (London), A236, 535 (1956).
52. S.M. Quick, M.Sc. Thesis, U. of Windsor (1966) (Unpublished).
53. F. Holuj, Can. J. Phys., 46, 287 (1968).
54. F.W. Ashton and R. Wilson, Am. J. Sci., 13, 209 (1927).
55. W.A. Pieczonka, H.E. Petch, and A.B. McLay, Can. J. Phys., 39, 145 (1961).
56. P.E. Halstead and A.E. Moore, J. Chem. Soc., (London), 3873 (1957).
57. R. Calvo and R. Orbach, Phys. Rev., 164, 284 (1967).

## APPENDIX A

Proton MR Frequencies Obtained in Calibration of Magnetic Field  
Across 6 in. Gap of Varian Magnet

Freq. (KHz) at pole face	Freq. (KHz) at gap center	Freq. (KHz) from formula	Freq. (KHz) at pole face	Freq. (KHz) at gap center	Freq. (KHz) from formula
11527.5	11446.8	11446.5	13819.7	13721.9	13721.9
11546.8	11465.9	11465.6	14040.4	13941.2	13940.9
11654.9	11573.4	11573.0	14250.0	14149.0	14149.0
11872.5	11789.1	11789.0	14468.5	14366.0	14365.9
12090.8	12005.9	12005.7	14683.9	14580.0	14579.7
12309.3	12222.8	12222.5	14898.8	14793.1	14793.0
12519.3	12431.0	12431.0	15114.1	15006.8	15006.8
12741.7	12652.0	12651.8	15330.1	15221.4	15221.2
12962.1	12870.6	12870.6	15546.7	15436.2	15436.2
13173.7	13080.8	13080.6	15761.4	14649.4	15649.3
13386.4	13291.3	13291.7	15979.1	15865.5	15865.4
13606.6	13510.4	13510.3	16192.6	16077.8	16077.3
			16498.3	16381.1	16380.8

Best fit data of spin-Hamiltonian parameters  $b_2^0$ ,  $b_4^0$ , A and B, and the quantities  $|(A^2-B^2)^{1/2}/A|$  and  $(A+2B)/3$  in gauss as a function of temperature.

T(°K)	$b_2^0$	$b_4^0$	A	B	$ (A^2-B^2)^{1/2}/A $	$(A+2B)/3$
84.0000	-16.0000	-2.2500	-93.1100	-91.3300	.1945	-91.9233
99.0000	-15.8500	-2.3000	-93.1500	-91.3500	.1956	-91.9500
106.0000	-15.7500	-2.3000	-93.1000	-91.3500	.1929	-91.9333
121.0000	-15.5000	-2.3000	-93.1000	-91.3500	.1929	-91.9333
133.0000	-15.1000	-2.3000	-93.0500	-91.3000	.1930	-91.8833
153.0000	-13.8000	-2.3000	-93.0000	-91.1000	.2011	-91.7333
171.0000	-13.0000	-2.3000	-92.8500	-91.0500	.1959	-91.6500
196.0000	-12.2200	-2.2800	-92.7200	-90.9000	.1971	-91.5066
225.0000	-10.6000	-2.3000	-92.6000	-90.6500	.2041	-91.3000
248.0000	-9.6000	-2.2500	-92.5500	-90.6500	.2015	-91.2833
276.0000	-8.1000	-2.2600	-92.2500	-90.4000	.1992	-91.0166
290.0000	-6.6000	-2.5400	-92.0500	-90.3000	.1940	-90.8833
322.0000	-5.0000	-2.1000	-91.6000	-90.2100	.1735	-90.6733
344.0000	-4.4000	-2.2600	-91.4800	-90.1000	.1730	-90.5600
377.0000	-.9000	-2.2000	-91.3000	-89.8900	.1750	-90.3600

APPENDIX B (continued)

401.0000	-1.6000	-2.1000	-91.2000	-89.7000	.1806	-90.2000
453.0000	1.0000	-2.2000	-90.6700	-89.4300	.1648	-89.8433
493.0000	2.0000	-2.4000	-90.5500	-89.1500	.1751	-89.6166
516.0000	4.0000	-2.5000	-90.4000	-88.9200	.1802	-89.4133
544.0000	4.8000	-2.5000	-90.1000	-88.7400	.1730	-89.1933
550.0000	6.2000	-2.2000	-90.1500	-88.8000	.1724	-89.2500
579.0000	7.0000	-2.2000	-89.9000	-88.7100	.1621	-89.1066
605.0000	7.8000	-2.5000	-89.8500	-88.6000	.1662	-89.0166
636.0000	10.0000	-2.2600	-89.7000	-88.3500	.1728	-88.8000
680.0000	12.0000	-2.3000	-89.4000	-88.2200	.1619	-88.6133
705.0000	12.6000	-2.2800	-89.3300	-87.9100	.1775	-88.3833
735.0000	13.0000	-2.3000	-89.1000	-87.7500	.1734	-88.2000
750.0000	13.8000	-2.3000	-89.0000	-87.6700	.1722	-88.1133
761.0000	15.2000	-2.3000	-89.0000	-87.6700	.1722	-88.1133
781.0000	16.9000	-2.2800	-88.8000	-87.7000	.1569	-88.0666

## VITA AUCTORIS

On August 1, 1942, I was born in Redhill, Surrey, England. In 1946, I emigrated to Essex county in Ontario where I graduated from S.S. No. 1 Public School, Maidstone, in 1956 and Essex District High School, in 1961. I received my university education at the University of Windsor, graduating with B.Sc. in 1965 and with M.Sc. in 1966.